The lysine deacetylase activity of HDAC1/2 is required to safeguard zygotic genome activation in mice and cattle

Yanna Dang[1,‡], Shuang Li[1,‡],Panpan Zhao[1‡,], Lieying Xiao[1], Lefeng Wang[1,2], Yan Shi[1], Lei Luo[1], Shaohua Wang[1], Huanan Wang[1,2] and Kun Zhang[1,*]

[1]Laboratory of Mammalian Molecular Embryology, College of Animal Sciences, and Assisted Reproduction Unit, Department of Obstetrics and Gynecology, Sir Run Run Shaw Hospital, School of Medicine, Zhejiang University, Hangzhou, Zhejiang 310058, China; [2]Department of Veterinary Sciences, College of Animal Sciences, Zhejiang University, Hangzhou, Zhejiang 310058, China;

[*]To whom correspondence may be addressed. Email: kzhang@zju.edu.cn

[‡]Y.D., S.L., and P.Z. contributed equally to this work.

Corresponding Author: Kun Zhang, Room 301 E Building, 866 Yuhangtang Rd, Hangzhou, Zhejiang 310058, China, Tel: 86-(571) 8898-2506; Email: kzhang@zju.edu.cn

Keywords: ZGA; Chromatin; Reprogramming; HDAC1/2; Preimplantation; Embryo

Summary statement

Upon fertilization, the activation of the new life's genome is a landmark developmental event. Here, we find HDAC1/2 are critical epigenetic modifiers that maintain the transcriptional states during zygotic genome activation.

ABSTRACT

The genome is transcriptionally inert at fertilization and must be activated through a remarkable developmental process called zygotic genome activation (ZGA). Epigenetic reprogramming contributes significantly to the dynamic gene expression during ZGA, however the mechanism has yet to be resolved. Here, we find histone deacetylase 1 and 2 (HDAC1/2) can regulate ZGA through the lysine deacetylase activity. Notably, in mouse embryos, overexpression of HDAC1/2 dominant negative mutant leads to a developmental arrest at 2-cell stage. RNA-seq reveals that 64% of down-regulated genes are ZGA genes and 49% of up-regulated genes are developmental genes. Inhibition of the deacetylase activity of HDAC1/2 causes a failure of histone deacetylation at multiple sites including H4K5, H4K16, H3K14, H3K18, and H3K27. ChIP-seq analysis exhibits an increase and decrease of H3K27ac enrichment at promoters of up- and down-regulated genes, respectively. Moreover, HDAC1 mutants prohibited the removal of H3K4me3 via impeding KDM5s. Importantly, the developmental block can be greatly rescued through *Kdm5b* injection and expression of the majority of dysregulated genes partially corrected. Similar functional significance of HDAC1/2 is conserved in cattle embryos. Overall, we propose that HDAC1/2 is indispensable for ZGA via creating correct transcriptional repressive and active states in mouse and bovine embryos.

INTRODUCTION

The highly differentiated germ cells (sperm and egg) go through the fertilization process to form a totipotent zygote, which marks the beginning of a new life. However, the new life must complete a developmental process called maternal zygotic transition (MZT) or oocyte-to-embryo transition (OET) to acquire its developmental independence(Schultz et al., 2018; Vastenhouw et al., 2019). During this transition, the genome is transcriptional quiescent initially and the development control relies on maternal derived transcripts and proteins. These maternal factors gradually undergo clearance while zygotic genome is activated (ZGA). ZGA typically occurs in two consecutive waves, termed minor and major ZGA. The timing of ZGA

varies among mammals. In mice, minor and major ZGA occurs in late one-cell and mid-to-late 2-cell embryos, respectively. The gene expression pattern established during ZGA is required for setting up totipotency in early embryos and the ensuing development. Therefore, a central question in biology is the defining feature of chromatin states during ZGA and how it contributes to changes in gene expression.

A considerable epigenetic reprogramming is a remarkable feature of early stage embryogenesis(Eckersley-Maslin et al., 2018; Du et al., 2021; Xu et al., 2021b). In particular, DNA methylations and various histone modifications are subject to dramatic remodeling, which is believed to ensure correct gene expression program and ZGA. Indeed, aberrant DNA methylation and histone modifications in fertilized or cloned embryos have been closely linked to abnormal gene expression and developmental failure(Matoba et al., 2014; Gao et al., 2018). However, studies of molecular mechanisms of epigenetic reprogramming is traditionally limited by the scarce samples and a lack of tools for chromatin analysis in early embryos.

With the rapid advance of low-input chromatin profiling methods including micro-scale ChIP-seq and CUT&RUN(Brind'Amour et al., 2015; Dahl et al., 2016; Liu et al., 2016; Zhang et al., 2016; Skene et al., 2018; Kaya-Okur et al., 2020), how histone modifications patterns are passed, reprogrammed, and established from oogenesis to early embryogenesis have been unveiled and their correlation with gene expression profiles determined(Dahl et al., 2016; Liu et al., 2016; Zhang et al., 2016; Xu et al., 2021a). However, the causal relationship between these histone modifications and gene expression as well as the crosstalk between histone modifications have yet to be resolved.

Histone acetylation is widely considered as a hallmark of active gene expression(Dahl et al., 2016). It has been shown that H3K9ac regulates the transition from transcription initiation to elongation(Gates et al., 2017). Importantly, insufficient H3K9ac act as an epigenetic barrier in mouse somatic cell nuclear transfer (SCNT) embryos(Yang et al., 2021). During oocyte maturation, aberrant increase of H4K16ac induces defective chromatin structure and impairs oocyte growth and development(Ma and Schultz, 2013; Zhang et al., 2014). As the most-characterized

histone acetylation, H3K27ac is associated with increased release of RNA polymerase II into active transcription and is typically accumulated at promoters and enhancers of active expressed genes(Creyghton et al., 2010). In zebrafish embryos, there is a global loss of H3K27ac marks at enhancers while widespread de novo H3K27ac is acquired at promoters prior to ZGA(Zhang et al., 2018). Therefore, these results indicate the importance of histone acetylation reprogramming in early embryonic development.

Histone acetylation is directly controlled by histone acetyltransferases (HATs) and histone deacetylases (HDACs)(Sheikh and Akhtar, 2019). Mutations of these enzymes often lead to embryonic lethality in mice and are connected with human diseases(Sheikh and Akhtar, 2019). HDAC1 is the first HDAC to be characterized. To date, four classes of 18 HDACs have been identified in mammals. Among them, class I family members (HDACs 1, 2, 3 and 8) display highest sequence homology to HDAC1 and ubiquitously expressed, localized in the nucleus, and exhibit high catalytic activity towards histone substrates. HDAC1 and HDAC2 are the top expressed HDACs in mouse oocytes and embryos(Dahl et al., 2016). Genetic evidence reveals an overlapping and essential role of HDAC1 and 2 during oogenesis(Ma et al., 2012). Previous research demonstrates an important role for *Hdac1* in preimplantation development in mice using a knockdown approach(Ma and Schultz, 2008). Moreover, our recent work established a redundant role of HDAC1 and HDAC2 in mouse early embryogenesis(Zhao et al., 2020). However, the specific role of HDAC1/2 in ZGA remains unclear given the technical difficulty in acutely removing maternal HDAC1/2.

In this study, we demonstrate that the lysine deacetylase activity of HDAC1/2 is required for ZGA in both mice and cattle by using a combination of dominant negative approach and pharmacological approach. HDAC1/2 mutants lead to a large-scale dysregulation of gene expression during ZGA and a developmental arrest at 2-cell stage. Mechanistically, HDAC1 mutants results in a deviant genome-wide distribution of histone acetylation and prohibits the removal of broad H3K4me3 domain by disrupting the expression of *Kdm5s*. Moreover, the developmental phenotype can be greatly rescued through injection of *Kdm5b* mRNA. We propose

that HDAC1/2 are critical epigenetic modifiers that maintain the transcriptional states during ZGA through their lysine deacetylase activity.

RESULTS

HDAC1/2 is essential for ZGA in both mouse and bovine embryos

To study the functional role of HDACs in ZGA, we first validated the expression pattern of HDACs in mouse and bovine embryos. Transcriptomic analysis revealed that *Hdac1*/*HDAC1* and *Hdac2*/*HDAC2* were the most abundant among all *Hdacs*/*HDACs* in both mouse (Fig. S1A) and bovine early embryos (Fig. S1B). In particular, *Hdac1* mRNA abundance increased gradually and visibly during ZGA in both species (Fig. S1A-B). In accordance with the mRNA change, the nuclear intensity of HDAC1 was increased during ZGA (Fig. S1C-D). These results suggest that HDAC1/2 might play a role during ZGA.

To delve into the function of HDAC1/2 in ZGA, we treated the zygotes with FK228, a HDAC1/2-specific inhibitor(Furumai et al., 2002). Embryo culture results showed FK228-treated embryos arrested at 2-cell stage in mice (Fig. S1E). Concomitantly, FK228 treatment resulted in a developmental arrest in cattle and cell number analysis with DAPI staining clarified that these embryos arrested at 8/16-cell stage (bovine ZGA; Fig. S1F-G).

To probe the specific effects of the lysine deacetylase activity of HDAC1, we generate a mutant in the lysine deacetylase domain. The lysine deacetylase domain conserved to all Class I HDACs consists of a stretch of more than 300 amino acids and a mutation in the amino acid sequence destroys its enzymatic activity(Hassig et al., 1998). We therefore constructed a HDAC1 mutant in which the residue histidine 141 (H141) was replaced by alanine, and the mutant can abolish deacetylase activity of HDAC1 by competitive inhibition without destroying the interaction with HDAC1-associated proteins(Hassig et al., 1998). The resultant mutant is referred to here as H1MU while the wild type is referred to as H1WT. We microinjected early zygotes with mRNA for H1WT and H1MU. H_2O was injected in control groups (Fig. 1A). Nearly all of the embryos in H1MU group suffered developmental arrest at 2-cell

stage (87%) while the control embryos exhibit robust development with 80% developing to blastocyst stage (Fig. 1A-C).

HDAC1 and 2 are two homologous histone deacetylases and exhibit functional redundancy in oogenesis and preimplantation development(Ma et al., 2012; Zhao et al., 2020). We therefore asked if these two proteins play a redundant role during ZGA. *Hdac2* mutant was also generated by employing a mutation in the catalytic domain(Kurita et al., 2012). Likewise, the mutation also caused embryonic arrest at 2-cell stage (Fig. 1D). Overall, these data revealed that HDAC1/2 is crucial for ZGA in both mouse and bovine embryos.

HDAC1 mutation results in aberrant gene expression pattern during ZGA

To gain insight into developmental failure of H1MU embryos at the molecular level, we measured the level of phospho-Ser2 (Ser2P), a hallmark of RNA polymerase II activity, to examine if the inhibition of HDAC1 affect the genome-wide transcriptional program, but there was no visible difference between H1MU and H1WT embryos (Fig. S2).

Furthermore, we collected early 2-cell embryos from H1WT, H1MU groups and late 2-cell stage embryos from H_2O, H1WT, and H1MU groups and performed RNA-seq (Fig. 2A). Two independent replicates for RNA-seq samples from each group displayed high correlation (Fig. S3A). In addition, *Hdac1* was significantly increased in both H1WT and H1MU groups, further confirming a robust overexpression efficiency (Table S2).

H1MU has no significant impact on minor ZGA as the analysis revealed only 77 and 60 up-regulated and down-regulated genes, respectively (*Padj* <= 0.05; Fold change >= 2 or <= 0.5) at early 2-cell stage in H1MU versus H1WT groups (Fig. 2B). Moreover, at late 2-cell stage, there are only 88 genes differentially expressed in WT groups compared with control groups, suggesting H1WT overexpression has minor effect on the transcriptome during ZGA (Fig. S3B). In contrast, 6565 genes were differentially expressed in late 2-cell embryos of H1MU compared to H1WT groups with 3898 and 2667 up-regulated and down-regulated genes, respectively (Fig. 2C

and Table S2). These transcriptomic comparisons at the two different embryonic stages clearly indicated HDAC1 specifically regulate gene transcription when major ZGA occurs.

Gene Ontology (GO) enrichment analysis of up-regulated genes revealed overrepresentation of genes involved in transcription and sequence-specific DNA binding (Table S3). Meanwhile, similar analysis of down-regulated genes showed that a significant number of genes were involved in transcription and RNA splicing, ribosome biogenesis and nucleotide metabolism, which are known markers of ZGA(Zeng and Schultz, 2005) (Table S4). We also noticed a drastic reduction of the expression of *Brg1/Smarca4*(Bultman et al., 2006) and *Nfya*(Lu et al., 2016)(Table S2), two genes known for their putative function in regulating mouse ZGA.

To assess the molecular feature of HDAC1's target genes, we then examine the expression pattern of the up-regulated genes and down-regulated genes during normal preimplantation development. We categorized the up-regulated and down-regulated genes into three main classes each by *k-means* clustering. Surprisingly, a considerable number of up-regulated genes are maternal (Cluster 1) and developmental genes (Cluster 3), which are supposed to be silent, while the majority of down-regulated genes are ZGA genes (Cluster 5; Fig. 2D-E). These results suggest HDAC1's enzymatic activity is required not only for transcriptional silencing but transcriptional activation during ZGA.

To address directly if there is functional redundancy for HDAC1/2 in regulating gene transcription, we compared differentially expressed genes (DEGs) caused by H1MU and H2MU. Results indicated that the majority of up-regulated and down-regulated genes are common to both groups (Fig. 2F and S3C), suggesting a compensatory role of HDAC1/2 in transcriptional regulation. We also observed FK228 treatment resulted in similar changes in the transcriptome (Fig. 2G, S3D-E), indicating its specificity in inhibiting the lysine deacetylase activity of HDAC1/2. In agreement with the result of H1MU, we observed the majority of up-regulated and down-regulated in H2MU or FK228-treated groups are maternal/developmental genes and ZGA genes, respectively (Fig. S3F-H). Besides, clustering analysis showed that the transcriptome of embryos

in H1MU, H2MU and FK228 group is distinguishable from those of wild type early 2-cell embryos, which demonstrated that the observed transcriptional changes are not due to developmental delay (Fig. S3E). Overall, these data confirmed the importance of HDAC1/2 for ZGA.

The lysine deacetylase activity of HDAC1/2 is required for reprogramming of histone acetylation during ZGA

Given the deacetylase activity of HDAC1/2, we sought to determine if HDAC1/2 mutation affects the reprogramming of histone acetylation. IF results showed a decrease of H3K27ac, H3K14ac, H3K18ac, H4K5ac and H4K16ac in H1WT embryos compared with those in H_2O-injected controls (Fig. 3A and S4A-D), confirming the effective overexpression of HDAC1. Importantly, we observed a robust increase of H3K27/K14/K18ac and H4K5/K16ac in H1MU embryos (Fig. 3A-B and S4A-D). We validated that similar changes for H3K27ac were found in FK228-treated group and H2MU groups (Fig. 3C-D and S4E-F). Hence, the developmental failure observed upon inhibition of HDAC1/2 might be ascribed to the aberrant histone acetylation reprogramming during ZGA.

The defective ZGA accompanied by hyperacetylation described above prompted us to explore the correlation between histone acetylation and ZGA. For this purpose, we measured the reprogramming of H3K27ac, which is a well-established marker of active chromatin in somatic cells. In mice, relatively strong signals of H3K27ac were detected in both maternal and paternal pronuclei at zygote stage and its nuclear intensity drastically diminished from the early and late 2-cell stages, concurrent with mouse major ZGA (Fig. 3E). In cattle, H3K27ac is still relatively bright at 4-cell stage, when minor ZGA occurs, however, it underwent a sharp decrease at 8- and 16-cell stage, coinciding with bovine major ZGA (Fig. 3F). These data are in agreement with previous studies in mice(Santenard et al., 2010) and such coincidence with ZGA was also reported in pigs(Zhou et al., 2014), suggesting that this global loss of histone acetylation is conserved in mammals.

HDAC1 mutation results in aberrant distribution of histone acetylation in early embryos

To explore the correlation between hyperacetylation and dysregulated gene expression upon the inhibition of HDAC1, we performed Ultra-Low-Input-NChIP-seq (ULI-NChIP-seq) of H3K27ac at late 2-cell stage and obtained high-quality reproducible data (Fig. 4A-B, and S5A). The protocol used here is highly efficient since our data in control groups faithfully recapitulates the previously published H3K27ac ChIP-seq data(Dahl et al., 2016) with a high correlation (R=0.80; Fig. S5B-C). Genome distribution of H3K27ac changed significantly in H1MU embryos. In particular, H3K27ac enrichment at promoter and distal regions were decreased and increased, respectively (Fig. 4C). By scanning the genome with a 5 kb sliding window, we identified H3K27ac-lost and -gained regions in H1MU embryos. In consistent with our IF results, H3K27ac-gained regions covered more genome than H3K27ac-lost regions (Fig. 4D).

To establish if the epigenetic changes associated with the transcriptomic differences, we profiled H3K27ac signal in promoters of up-regulated and down-regulated genes. H3K27ac was accumulated in both promoters and gene bodies of up-regulated genes in H1MU group (Fig. 4E and S5D). On the contrary, the promoters and gene bodies of down-regulated genes displayed reduced H3K27ac signal (Fig. 4F and S5E). These results suggest that the disorder of gene expression pattern caused by H1MU is correlated with the aberrant histone deacetylation.

DUX is up-regulated upon HDAC1 mutation

To identify sequence motifs for DNA-binding proteins that were potentially enriched in aberrant H3K27ac-deposited regions, we scanned the entire genome within a 1 kb window to calculate H3K27ac signals, and annotated motifs at the top 2% H3K27ac-increased and -decreased regions by HOMER. Notably, DUX was significantly enriched in the H3K27ac-increased regions (Fig. 5A). However, these motifs were not detected in H3K27ac-decreased regions. Altogether, these results

suggest that H1MU influences expression of active and repressed genes through distinct regulatory mechanisms.

DUX (DUX4 in humans) is a putative transcriptional factor involved in regulation of mammalian ZGA(De Iaco et al., 2017; Hendrickson et al., 2017; De Iaco et al., 2020). *Dux* is supposed to be transiently expressed during early to mid-2-cell stage and rapidly disappears at late 2-cell stage (Fig. 5B)(Guo et al., 2019). However, although there was a distinct decrease of *Dux* in late 2-cell embryos of H1MU groups, the amount was still greater than that in control embryos (Fig. 5B). *Zscan4s* and *ERVLs* are identified as target genes of DUX, and can be robustly expressed in mouse embryos overexpressing DUX(Guo et al., 2019). We found the expression of *Zscan4s* and *ERVLs (MERVL-int and MT2_mm)* was also increased in H1MU embryos (Fig. 5C, 5D and 5E). Therefore, it is highly possible that the insufficient repression of *Dux* is one leading factor causing the up-regulation of repressed genes, including developmental and maternal genes.

It has been reported that DUX4 function as a DNA-binding protein that recruits EP300/CBP through its C-terminals to activate expression of nearby genes(Choi et al., 2016). Intriguingly, the average mRNA abundance of up-regulated genes in late 2-cell H1WT embryos is lower than those of down-regulated genes (Fig. 5F), suggesting the timely loss of DUX in late 2-cell embryos is critical to maintain the low expression of those up-regulated genes.

HDAC1 mutation inhibits the removal of broad H3K4me3 domain during mouse ZGA

H3K4me3 is an established hallmark of permissive promoters that can tether chromatin remodelers and transcriptional regulators. Genome-wide distribution of H3K4me3 is unique in early embryos for its broad domains established during oogenesis and removed upon ZGA(Dahl et al., 2016; Liu et al., 2016; Zhang et al., 2016). Next, we wondered if H3K4me3 reprogramming was affected in H1MU embryos. We observed a notable level of H3K4me3 at early 2-cell stage in control groups and no difference was found in H1MU groups (Fig. S6A). Furthermore,

H3K4me3 signal can be barely seen in control embryos while the intensity was obviously increased in H1MU embryos at late 2-cell stage, suggesting the removal of broad H3K4me3 domain is blocked (Fig. 6A-B). In consistent with H1MU's effect, we also found the erasure of broad H3K4me3 domain was suppressed when H2MU or FK228 treatment was employed (Fig. S6B-D).

We then analyzed the global dynamics of H3K4me3 in H1MU and control embryos by ChIP-seq. We validated the H3K4me3 ChIP first and found there is high correlation between our data in control groups and the previously published H3K4me3 ChIP-seq data(Zhang et al., 2016) (R=0.81; Fig. S7A-B). The two biological replicates for both groups exhibit high correlation, indicating a high reproducibility (Fig. S7C-D). We identified 34590 H3K4me3-gained domains and 5890 H3K4me3-lost domains in H1MU embryos, which covered 4.5% and 0.7% of the genome respectively. Moreover, H3K4me3-gain regions accounted for nearly 50% at distal regions while H3K4me3-lost regions accounted for 25% at distal regions, further suggesting a block in removal of broad H3K4me3 domain (Fig. 6C).

H3K4me3 reprograming is critical to ensure gene expression program during ZGA. We therefore sought to determine if H3K4me3 involved in transcriptomic changes in H1MU embryos. Surprisingly, H3K4me3 was reduced at promoters of both up- and down-regulated genes in H1MU group (Fig. 6D-G). However, H3K4me3 signals were enhanced in gene body regions of up-regulated genes while it was reduced at gene body regions of down-regulated genes (Fig. 6D-G), suggesting that the dysregulated gene expression could be ascribed to the sustained broad H3K4me3 domain. Altogether, HDAC1's enzymatic activity is crucial for the immediate removal of broad H3K4me3 domain upon ZGA.

Broad H3K4me3 domains are removed by KDM5 family members during mouse ZGA(Dahl et al., 2016; Liu et al., 2016; Zhang et al., 2016). Interestingly, GO analysis of down-regulated genes revealed genes involved in histone H3-K4 demethylation (Table S4). Indeed, mRNA abundance of all three *Kdm5s (Kdm5a, 5b, 5c)* was dramatically decreased in H1MU embryos (Fig. 6H). *Kdm5b* is zygotic transcribed from early to late-2 cell stage (Fig. S7E) while H3K27ac is accumulated at

Kdm5b (Fig. 6I). In contrast, H1MU caused a reduction in H3K27ac enrichment at *Kdm5b* (Fig. 6J), suggesting H3K27ac regulates transcription of *Kdm5b*.

KDM5B is a key mediator of the HDCA1 MU phenotype

We next asked if ectopic injection of *Kdm5* mRNA could rescue the H3K4me3 pattern and the developmental outcome of H1MU embryos (Fig. 7A). Because *Kdm5b* normally begins its transcription at 2-cell stage, we thus performed microinjection of *Kdm5b* mRNA into two individual blastomeres of early 2-cell embryos. Results showed microinjection of *Kdm5b* resulted in a significant decrease of global H3K4me3 in H1MU embryos, indicating a recovery of H3K4me3 reprogramming (Fig. 7B). As a consequence, the majority of the co-injected embryos could overcome the 2-cell block (Fig. 7C-D), with 46% develop to 4/8-cell stage and 14% even can develop to morula stage (Fig. S7F). RNA-seq analysis revealed that the expression of 53.99% of downregulated genes and 42.21% of upregulated genes in H1MU groups could be at least partially corrected by ectopic expression of *Kdm5b* (Fig. 7E), and the rescued genes were significantly enriched in major ZGA (Fig. 7F), suggesting that the accurate distribution of H3K4me3 is required for ZGA. Remarkably, expression of *Dux* dropped to normal levels when overexpressed KDM5B, and its targets *Zscan4s* were also reduced greatly (Fig. 7G-H), suggesting that HDAC1 regulates DUX through KDM5B. Together, these findings implicate KDM5B as a key molecular mediator of HDAC1 function in controlling H3K4me3 reprogramming.

Function of HDAC1 on ZGA is conserved in mouse and bovine embryos

Recent studies in epigenome reprogramming have revealed remarkable differences among mammals(Hanna et al., 2018; Xia et al., 2019). To determine if the effect of HDAC1 on transcriptional regulation during ZGA is conserved, we collected DMSO and FK228-treated 8-16 cell embryos and performed RNA-seq. We identified 1990 and 2794 up-regulated and down-regulated genes, respectively (Fig. 8A-B and S8A-B). 74% (2061/2794) of the down-regulated genes are supposed to be expressed at 8/16-cell stage (Fig. 8B-C and S8B-C), indicating a ZGA defect. Strikingly, *KDM5s*

were repressed in FK228-treated embryos (Fig. 8D), which is accompanied by an increase of H3K4me3 during ZGA (Fig. 8E-F). Furthermore, we microinjected *H1MU* mRNA to bovine zygotes (Fig. S8D) and found similar results with FK228 experiment. Most of the H1MU embryos were arrested at 8/16-cell stage (Fig. S8D-E) with an obvious increase of H3K27ac and H3K4me3 compared with control embryos (Fig. S8F-G). In summary, these results suggested that HDAC1/2 plays a conserved role in regulation of gene expression pattern during ZGA.

DISCUSSION

A fundamental question in developmental biology is what factors trigger ZGA in mammals. Accumulative evidence has revealed a growing list of proteins involved in the process(Bultman et al., 2006; Lu et al., 2016; De Iaco et al., 2017; Hendrickson et al., 2017). However, the molecular mechanisms of ZGA have yet to be determined. (Mal et al., 2001; Humphrey et al., 2008). Here, we demonstrate that the lysine deacetylase activity of HDAC1/2 is critical for establishing correct gene expression profile during ZGA. Mechanistically, HDAC1/2 regulates gene expression likely through controlling the reprogramming of histone acetylation and H3K4me3. Importantly, HDAC1 acts as an upstream factor of KDM5B to regulate expression of target genes. We propose that HDAC1/2 is not only involved in development of the transcriptional repressive state for repressed genes but transcriptional active state for ZGA genes. To our knowledge, HDAC1/2 represent the first proteins hold a dual role in transcriptional regulation during ZGA.

We demonstrated that the lysine deacetylase activity of HDAC1/2 is responsible for development progression throughout ZGA. In agreement with our data, previous reports show that HDAC1 is zygotically expressed beginning from 2-cell stage and only HDAC1 is sensitive to α-amanitin among the HDACs expressed in 2-cell embryos(Zeng and Schultz, 2005; Dahl et al., 2016). Upon fertilization, HDAC1 seems one of key molecular players directly involved in development of transcriptional repressive state for maternal and developmental genes. Indeed,

inhibition of HDAC1 leads to up-regulated expression of 3898 genes and the majority of them belong to maternal and developmental genes.

Interestingly, we further identified *DUX* was aberrantly up-regulated upon HDAC1 mutation. As an intron-less and multi-copy gene that encodes a double-homeobox transcriptional factor involved in major ZGA, *Dux* is transiently transcribed during minor ZGA and its timely removal is critical for early embryogenesis(Guo et al., 2019), of which the biological significance remains unclear. It is possible that the DUX removal is critical to inhibit the transcription activity for those up-regulated genes induced by HDAC1 mutation. Indeed, human DUX4 can recruit EP300 through its C-terminals and therefore involved in histone acetylation(Choi et al., 2016; Bosnakovski et al., 2019). However, it warrants further investigation on how HDAC1/2 regulates DUX expression.

Histone acetylation has long been linked with transcriptional permissive state. We observed a sharp decrease of global H3K27ac in both mouse and cattle. This phenomenon also occurs to other histone acetylation during ZGA in mice, cattle, and pigs(Santenard et al., 2010; Zhou et al., 2014), suggesting histone deacetylation is a conserved event to set up chromatin state prior to ZGA. Hence, we speculate that histone deacetylation is one upstream inducer of the major ZGA since it occurs prior to the major ZGA and earlier than H3K4me3 reprogramming (early to late 2-cell stage), which appears as a ZGA regulator(Dahl et al., 2016). Indeed, HDAC1/2 mutant elicits a dramatic downregulation of ZGA genes. These genes account for 24% of all ZGA genes. Interestingly, H3K27ac was decreased at promoters of these genes after H1MU injection, in contrasting with HDAC1's deacetylase activity. Thus, HDAC1 may regulate transcriptional activity of these active genes in an indirect manner, which awaits additional investigation.

Crosstalk of different epigenetic modifications makes up precise regulatory network for gene expression(Eckersley-Maslin et al., 2018; Xu and Xie, 2018). KDM5s were down-regulated in embryos injected with mutant *Hdac1* mRNA and caused inadequate removal of broad H3K4me3 in gene body and intergenic regions. Timely removal of broad H3K4me3 is viewed associated with mouse ZGA, but

Kdm5s-knockdown embryos can develop beyond ZGA although a set of ZGA genes were slightly down-regulated at 2-cell stage(Dahl et al., 2016; Liu et al., 2016), suggesting that abnormal H3K4me3 alone plays limited roles in ZGA. However, the inhibition of HDAC1 could cause insufficient removal of histone acetylation and H3K4me3 concurrently, and led to developmental arrest at 2-cell stage. Surprisingly, the injection of exogenous *KDM5B* mRNA could partly rescue the development of HDAC1 mutant embryos, suggesting that the role of HDAC1/2 in ZGA is at least partly mediated through regulation of H3K4me3 reprogramming.

Previous studies have shown HDAC1/2's substrates include not only histones but also non-histones(Luo et al., 2000; Nalawansha et al., 2017). Here, we found that HDAC1/2's activity is required for deacetylation at certain lysine sites of histones. In particular, we determined the changes in H3K27ac given its well-established association with active gene expression. However, we cannot rule out the possibility that the inhibition of HDAC1/2 could potentially affect other substrates, including non-histones, which warrants further investigations in the future.

Altogether, we demonstrate an indispensable role for the lysine deacetylase activity of HDAC1/2 for ZGA in both mice and cattle. HDAC1/2 is required for the proper reprogramming of histone acetylation and H3K4me3. The chromatin reprograming is critical for the development of both transcriptional repressive state for silent genes and transcriptional active state for ZGA genes.

MATERIALS AND METHODS

Ethics Statement

All procedures involving laboratory animals were carried out in accordance with the guidelines for the care and use of laboratory animals and approved by Zhejiang University.

Mouse embryo collection and in vitro culture

All experimental mice were raised and housed in a temperature controlled room (22-25˚C) with a relative humidity of 60% in a 12 hrs light/dark cycle in Laboratory Animal Center at Zhejiang University. All mice were provided access to food and water ad libitum. Eight to ten-week-old female BDF1 (C57BL/6 × DBA/2; Beijing Vital River Laboratory Animal Technology Co., Ltd.) mice were super-ovulated by an intraperitoneal injection of 7.5-10 IU PMSG (Sansheng Pharmaceutical Co. Ltd., Ningbo, China). Two days later, 7.5-10 IU hCG (Sansheng Pharmaceutical Co. Ltd., Ningbo, China) were administrated and mated with BDF1 male mice. 17-19 hrs after hCG injection, mice were sacrificed and zygotes were collected from the swollen upper part of the oviduct. Zygotes were incubated in the hyaluronidase (Sigma) solution to remove the cumulus cells and subsequently cultured in KSOM (Millipore) micro-drops under mineral oil at the condition of 37°C and 5% CO_2.

Bovine embryos *in vitro* production

Procedures of bovine *in vitro* production including *in vitro* maturation (IVM), *in vitro* fertilization (IVF) and *in vitro* culture (IVC) was carried out routinely in accordance with previously published studies(Wang et al., 2020; Shi et al., 2021). Briefly, cumulus-oocyte complexes (COCs) with >3 layers of cumulus cells were collected from ovaries derived from a local slaughterhouse. IVM was conducted with Medium-199 (M4530) supplemented with 10% FBS (Gibco-BRL, Grand Island, NY), 1 IU/ml FSH (Sansheng Biological Technology, Ningbo, China), 0.1 IU/ml LH (Solarbio, Beijing, China), 1 mM Na Pyruvate (Thermo Fisher Scientific, Waltham, MA), 2.5 mM GlutaMAX (Thermo Fisher Scientific, Waltham, MA), and 10 μg/mL Gentamicin. The IVM condition was 38.5°C under 5% CO_2 in humidified air for 22-24 hrs. IVF was performed by incubating COCs (60-100 COCs per well in 4-well plates) with spermatozoa ($1\sim5\times10^6$), which was purified from frozen-thawed semen by using a Percoll gradient in BO-IVF medium (IVF bioscience, Falmouth, Cornwall, UK). IVF condition was 38.5°C under 5% CO_2 for 9-12 hrs. Then, putative zygotes were removed of cumulus cells by pipetting up and down in Medium-199 (M7528)

supplemented with 2% FBS (Gibco-BRL, Grand Island, NY). Embryos were cultured in BO-IVC medium (IVF bioscience, Falmouth, Cornwall, UK) at 38.5°C under 5% CO_2 in humidified air until use.

FK228 treatment experiments

Romidepsin (FK228, Depsipeptide, Selleck) dissolved in dimethyl sulfoxide (DMSO, Sigma) was added to KSOM (for mice embryo) or BO-IVC medium (for bovine embryo) at a final concentration of 50 nM. In control group, equivalent amount of DMSO (0.1%) was added.

***In vitro* transcription and microinjection**

Wild-type or mutant cDNA for *Hdac1*, *Hdac2* and *Kdm5b* were subcloned into T7-driven vectors. *Hdac1* mutant (H141A) and *Hdac2* mutant (H141A) were constructed as described previously (Ito et al., 2002; Kurita et al., 2012). All sequences were validated by Sanger sequencing prior to use (Sangon, Shanghai, China). To prepare mRNAs for microinjection, the plasmids were linearized and *in vitro* transcribed, capped and poly(A) tailed using T7 mMESSAGE mMACHINE Ultra Kit (Life Technologies, Grand Island, NY, USA) according to the manufacturer's manual. RNA was recovered and purified by phenol:chloroform extraction and the integrity validated by gel electrophoresis.

mRNAs were microinjected into the cytoplasm of zygote 20-22 hrs post hCG injection using a Piezo-drill (Eppendorf, Germany) and Eppendorf transferman micromanipulators. *Hdac1* WT/mutant mRNA (500 ng/µl) or *Kdm5b* mRNA (1 µg/µl) was loaded into microinjection needle and a constant flow was adjusted in order to achieve successful microinjection. Around 10 pl of mRNA was microinjected into the cytoplasm of zygotes or 2 cell blastomere.

Immunofluorescence

Embryos were collected, washed and fixed for 10 minutes at room temperature in 4% formaldehyde in PBS (mouse: 10 min; cattle: 30 min). Embryo permeabilization was performed by treating with 0.5% Triton X-100 in PBS for 30 minutes in mice and 1 h in cattle. Then embryos were blocked in 10% fetal bovine serum in PBS for 1 h, and incubated in primary antibody for at least 1 h or 4°C overnight. After 3 washes with 0.1% Triton X-100 in PBS, fixed embryos were incubated with secondary antibodies for at least 1 h. DNA was counterstained with DAPI to locate the nuclear region. Embryos were imaged with Zeiss LSM 880 confocal microscope. All the antibodies used in the present study were listed in Table S1.

RNA-seq library preparation and sequencing

Mouse early 2-cell and late 2-cell stage embryos (50 embryos/sample, n=2 biological replicates/group) were collected at 24 h and 36 h post fertilization, respectively. Bovine 8/16-cell stage embryos (30 embryos/sample, n=2) were collected at 72 h post fertilization. Total RNA was extracted using Arcturus PicoPure RNA Isolation Kit (Life Technologies, Grand Island, NY, USA) according to the manufacturer's manual. Then mRNAs were separated using oligo(dT)25 beads. Sequencing libraries were constructed by using NEB Next Ultra RNA Library Prep Kit for Illumina (E7530) based on the instruction. Briefly, mRNAs were fragmented and reverse transcribed. cDNA library underwent end repair, poly(A)-tailing, adaptor ligation, and PCR amplification for 12–15 cycles in order to prepare the sequencing libraries. Paired-end 150 bp sequencing was performed on a NovaSeq (Illumina) platform by Novogene Co., Ltd.

ULI-NChIP-seq library preparation and sequencing

Mouse late 2-cell embryos (120 embryos/sample, n=2) were collected at 48 hrs after hCG injection. The zona pellucidae of the embryos were removed with Acid Tyrode's solution, then the embryos were washed 3 times in 0.5% bovine serum albumin (Millpore) in DPBS (Gibco) before flash-freezing in liquid nitrogen. ULI-NChIP was

performed according to the published protocols with slight modifications(Brind'Amour et al., 2015). One microgram of H3K4me3 (Cell Signaling Technology, #9751) or H3K27ac (Active Motif, AM39133) antibody was used for each immunoprecipitation reaction. ULI-NChIP-seq libraries were generated using the NEB Ultra DNA Library Prep Kit (E7645) according to the manual. Paired-end 150 bp sequencing was performed on a NovaSeq (Illumina) platform by Novogene Co., Ltd.

RNA-seq data alignment and quantification

The raw sequencing reads were trimmed with Trimmomatic (version 0.39)(Bolger et al., 2014) to get rid of low-quality reads and adaptor sequences. Clean reads were then mapped to mm10 (mouse) or ARS-UCD1.2 (bovine) with Hisat2 (version 2.1.0)(Kim et al., 2015). The raw read counts of genes were calculated with featureCounts (version 1.6.3)(Liao et al., 2014). For quantification of repetitive element, repeat annotations were downloaded from UCSC genome browser, and the raw counts of repetitive element were counted with BEDTools (version 2.30.1)(Quinlan, 2014). Gene expression values were normalized to FPKM with Cufflinks (version 2.2.1)(Trapnell et al., 2012) for heatmap, line plot and bar plot visualization. The raw counts of repetitive elements were normalized with DESeq2(Love et al., 2014) and then used for box pot visualization.

Differential expression analysis and functional annotation

Reads counts from FeatureCounts (genes) or BEDTools (repetitive elements) were used for differential expression analysis with DESeq2. The differentially expressed genes or repetitive elements between groups were identified when fold change >2 or <0.5 and adjusted *P* value < 0.05. The differential expression of repetitive elements was further validated by TEtranscripts python package (version 2.2.1)(Jin et al., 2015). Functional annotation and enrichment analysis of differentially expressed genes was performed with the Database for Annotation, Visualization and Integrated Discovery (DAVID)(Huang da et al., 2009a; Huang da et al., 2009b).

Classification of gene sets and clustering analysis

RNA-seq data of mouse and bovine oocytes and embryos was obtained from Jingyi Wu *et al.* (Wu et al., 2016)and Alexander Graf *et al*(Graf et al., 2014), respectively. The FPKM matrixes were generated with Cufflinks as described in RNA-seq data alignment and quantification section. Then the non-zero FPKM of genes was used for *k*-means clustering, which was performed with R based on Euclidean distance. After *k*-means clustering, genes with similar expression pattern were classified as maternal, minor ZGA, major ZGA or developmental genes. Clustering of differentially expressed genes was also performed as above. For hierarchical clustering of mouse late 2-cell embryos in different groups, euclidean distance of samples was calculated based on FPKM matrixes and hierarchical clustering was performed with hclust (dist, method = 'average') in R (http://www.rproject.org).

ChIP-seq data processing

The raw sequencing reads were trimmed with Trimmomatic (version 0.39)(Bolger et al., 2014) to remove residual adapter sequences and low-quality reads. Then the clean reads were aligned to mm10 using Bowtie2 (version 2.3.5)(Langmead and Salzberg, 2012) with default parameters. Alignments with low mapping quality were discarded by SAMtools (version 1.7)(Li et al., 2009), and PCR duplicates were removed with Picard (version 2.23; https://broadinstitute.github.io/picard/). To visualize H3K4me3 and H3K27ac signal in IGV genome browser, the genome was binned into 50 bp windows and RPKM for each window was calculated using bamCoverage function from DeepTools(Ramirez et al., 2014).

Correlation between biological replicates

The genome was binned into 2000 bp windows using makewindows utility of BEDTools(Quinlan and Hall, 2010), and the reads counts of each window were calculated and normalized to RPKM. Then the RPKM value for each sample was used to calculate Pearson correlation coefficient and draw scatter plots with R (http://www.rproject.org).

ChIP-seq peak calling

The peak number is affected by sequencing depth and equal numbers of ChIP and input reads result in best performance of peak callers(Chen et al., 2012; Jung et al., 2014). Therefore, we merged alignments of biological replicates and randomly subsampled them to equivalent depth using SAMtools before peak calling. The peaks were called by MACS2 (version 2.2.7.1)(Zhang et al., 2008) using the following parameters: -B -p 1e-5 --nomodel --broad --extsize 73. The peaks with fold enrichment less than 2 were removed. The filtered peaks were then annotated using ChIPseeker(Yu et al., 2015).

Identification of H3K27ac and H3K4me3-gained or -lost regions

To compared H3K27ac or H3K4me3 signals between groups, the mouse genome was scanned using a sliding window of 5 kb and step size of 1 kb, and then RPKM for each window was calculated. Next, H3K27ac or H3K4me3 signals were compared parallelly between H_2O and *Hdac1* MU. The H3K27ac and H3K4me3-gained or -lost regions were identified with following threshold: log2 (fold change) > 1.5 for gained regions or < -1.5 for lost regions, and sum of RPKM in H_2O and *Hdac1* MU >1. Then the selected regions were merged with BEDTools if they were overlapped, and the genome coverage of merged regions was calculated by genomecov mode of BEDTools.

Motif analysis

The mouse genome was first scanned using a sliding window of 1 kb and step size of 1 kb, and then RPKM of H3K27ac for each window was calculated. Next, the ratio of H3K27ac signal in *Hdac1* MU to H_2O was calculated, and windows with top 2% of ratios were retained as the most increased H3K27ac regions. On the other hand, windows with top 2% of ratios of H_2O to *Hdac1* MU were retained as the most decreased H3K27ac regions. The selected increased or decreased regions were merged with BEDTools if they were overlapped. The merged regions were used for

motif identification by Homer (version 4.11; http://homer.ucsd.edu/homer/motif/) with the parameters: -size given -p 10 -len 8.

Statistical analyses

Three biological replicates were conducted unless stated. Two-tailed unpaired Student's t test were performed to compare differences between groups. Immunofluorescent intensities were measured with ImageJ. Figures were generated by using GraphPad Prism 8 (GraphPad Software). Value of $P < 0.05$ denotes statistical significance. Results are shown as means ± SEM.

Acknowledgments

We thank Dr. Li Shen and Dr. Xudong Fu for their helpful discussions. Thank Dr. Zhe Zhang from Yuchun Pan's lab for their help on bioinformatic analysis.

Competing interests

The authors declare no competing interests.

Funding

This project was supported by National Natural Science Foundation of China [No. 31672416, No. 31872348, and No. 32072731 to K.Z.; No.31941007 to L.L. and S.W.; No. 32072939 to H.W.] and Zhejiang Provincial Natural Science Foundation [LZ21C170001 to K.Z. and No. LY19C180002 to H.W.] and China Postdoctoral Science Foundation [No. 2020M671742 to L.L.].

Data availability

Previously published datasets used in the present work include H3K27ac ChIP-seq (GSE72784:(Dahl et al., 2016)), H3K4me3 ChIP-seq (GSE71434:(Zhang et al.,

2016)), Mouse RNA-seq (GSE66582:(Wu et al., 2016)), and Bovine RNA-seq (GSE52415:(Graf et al., 2014)). Our RNA-seq and ULI-NChIP-seq data have been deposited to GEO with the accession number GSE182555.

References

Bolger, A. M., Lohse, M. and Usadel, B. (2014) 'Trimmomatic: a flexible trimmer for Illumina sequence data', *Bioinformatics* 30(15): 2114-20.

Bosnakovski, D., da Silva, M. T., Sunny, S. T., Ener, E. T., Toso, E. A., Yuan, C., Cui, Z., Walters, M. A., Jadhav, A. and Kyba, M. (2019) 'A novel P300 inhibitor reverses DUX4-mediated global histone H3 hyperacetylation, target gene expression, and cell death', *Sci Adv* 5(9): eaaw7781.

Brind'Amour, J., Liu, S., Hudson, M., Chen, C., Karimi, M. M. and Lorincz, M. C. (2015) 'An ultra-low-input native ChIP-seq protocol for genome-wide profiling of rare cell populations', *Nat Commun* 6: 6033.

Bultman, S. J., Gebuhr, T. C., Pan, H., Svoboda, P., Schultz, R. M. and Magnuson, T. (2006) 'Maternal BRG1 regulates zygotic genome activation in the mouse', *Genes Dev* 20(13): 1744-54.

Chen, Y., Negre, N., Li, Q., Mieczkowska, J. O., Slattery, M., Liu, T., Zhang, Y., Kim, T. K., He, H. H., Zieba, J. et al. (2012) 'Systematic evaluation of factors influencing ChIP-seq fidelity', *Nat Methods* 9(6): 609-14.

Choi, S. H., Gearhart, M. D., Cui, Z., Bosnakovski, D., Kim, M., Schennum, N. and Kyba, M. (2016) 'DUX4 recruits p300/CBP through its C-terminus and induces global H3K27 acetylation changes', *Nucleic Acids Res* 44(11): 5161-73.

Creyghton, M. P., Cheng, A. W., Welstead, G. G., Kooistra, T., Carey, B. W., Steine, E. J., Hanna, J., Lodato, M. A., Frampton, G. M., Sharp, P. A. et al. (2010) 'Histone H3K27ac separates active from poised enhancers and predicts developmental state', *Proc Natl Acad Sci U S A* 107(50): 21931-6.

Dahl, J. A., Jung, I., Aanes, H., Greggains, G. D., Manaf, A., Lerdrup, M., Li, G., Kuan, S., Li, B., Lee, A. Y. et al. (2016) 'Broad histone H3K4me3 domains in mouse oocytes modulate maternal-to-zygotic transition', *Nature* 537(7621): 548-552.

De Iaco, A., Planet, E., Coluccio, A., Verp, S., Duc, J. and Trono, D. (2017) 'DUX-family transcription factors regulate zygotic genome activation in placental mammals', *Nature Genetics* 49(6): 941-+.

De Iaco, A., Verp, S., Offner, S., Grun, D. and Trono, D. (2020) 'DUX is a non-essential synchronizer of zygotic genome activation', *Development* 147(2).

Du, Z., Zhang, K. and Xie, W. (2021) 'Epigenetic Reprogramming in Early Animal Development', *Cold Spring Harb Perspect Biol*.

Eckersley-Maslin, M. A., Alda-Catalinas, C. and Reik, W. (2018) 'Dynamics of the epigenetic landscape during the maternal-to-zygotic transition', *Nat Rev Mol Cell Biol* 19(7): 436-450.

Furumai, R., Matsuyama, A., Kobashi, N., Lee, K. H., Nishiyama, M., Nakajima, H., Tanaka, A., Komatsu, Y., Nishino, N., Yoshida, M. et al. (2002) 'FK228 (depsipeptide) as a natural prodrug that inhibits class I histone deacetylases', *Cancer Res* 62(17): 4916-21.

Gao, R., Wang, C., Gao, Y., Xiu, W., Chen, J., Kou, X., Zhao, Y., Liao, Y., Bai, D., Qiao, Z. et al. (2018) 'Inhibition of Aberrant DNA Re-methylation Improves Post-implantation Development of Somatic Cell Nuclear Transfer Embryos', *Cell Stem Cell* 23(3): 426-435 e5.

Gates, L. A., Shi, J., Rohira, A. D., Feng, Q., Zhu, B., Bedford, M. T., Sagum, C. A., Jung, S. Y., Qin, J., Tsai, M. J. et al. (2017) 'Acetylation on histone H3 lysine 9 mediates a switch from transcription initiation to elongation', *J Biol Chem* 292(35): 14456-14472.

Graf, A., Krebs, S., Zakhartchenko, V., Schwalb, B., Blum, H. and Wolf, E. (2014) 'Fine mapping of genome activation in bovine embryos by RNA sequencing', *Proc Natl Acad Sci U S A* 111(11): 4139-44.

Guo, M., Zhang, Y., Zhou, J., Bi, Y., Xu, J., Xu, C., Kou, X., Zhao, Y., Li, Y., Tu, Z. et al. (2019) 'Precise temporal regulation of Dux is important for embryo development', *Cell Res* 29(11): 956-959.

Halstead, M. M., Ma, X., Zhou, C., Schultz, R. M. and Ross, P. J. (2020) 'Chromatin remodeling in bovine embryos indicates species-specific regulation of genome activation', *Nat Commun* 11(1): 4654.

Hanna, C. W., Demond, H. and Kelsey, G. (2018) 'Epigenetic regulation in development: is the mouse a good model for the human?', *Human Reproduction Update* 24(5): 556-576.

Hassig, C. A., Tong, J. K., Fleischer, T. C., Owa, T., Grable, P. G., Ayer, D. E. and Schreiber, S. L. (1998) 'A role for histone deacetylase activity in HDAC1-mediated transcriptional repression', *Proc Natl Acad Sci U S A* 95(7): 3519-24.

Hendrickson, P. G., Dorais, J. A., Grow, E. J., Whiddon, J. L., Lim, J. W., Wike, C. L., Weaver, B. D., Pflueger, C., Emery, B. R., Wilcox, A. L. et al. (2017) 'Conserved roles of mouse DUX and human DUX4 in activating cleavage-stage genes and MERVL/HERVL retrotransposons', *Nat Genet* 49(6): 925-934.

Huang da, W., Sherman, B. T. and Lempicki, R. A. (2009a) 'Bioinformatics enrichment tools: paths toward the comprehensive functional analysis of large gene lists', *Nucleic Acids Res* 37(1): 1-13.

Huang da, W., Sherman, B. T. and Lempicki, R. A. (2009b) 'Systematic and integrative analysis of large gene lists using DAVID bioinformatics resources', *Nat Protoc* 4(1): 44-57.

Humphrey, G. W., Wang, Y. H., Hirai, T., Padmanabhan, R., Panchision, D. M., Newell, L. F., McKay, R. D. and Howard, B. H. (2008) 'Complementary roles for histone deacetylases 1, 2, and 3 in differentiation of pluripotent stem cells', *Differentiation* 76(4): 348-56.

Ito, A., Kawaguchi, Y., Lai, C. H., Kovacs, J. J., Higashimoto, Y., Appella, E. and Yao, T. P. (2002) 'MDM2-HDAC1-mediated deacetylation of p53 is required for its degradation', *EMBO J* 21(22): 6236-45.

Jin, Y., Tam, O. H., Paniagua, E. and Hammell, M. (2015) 'TEtranscripts: a package for including transposable elements in differential expression analysis of RNA-seq datasets', *Bioinformatics* 31(22): 3593-9.

Jung, Y. L., Luquette, L. J., Ho, J. W., Ferrari, F., Tolstorukov, M., Minoda, A., Issner, R., Epstein, C. B., Karpen, G. H., Kuroda, M. I. et al. (2014) 'Impact of sequencing depth in ChIP-seq experiments', *Nucleic Acids Res* 42(9): e74.

Kaya-Okur, H. S., Janssens, D. H., Henikoff, J. G., Ahmad, K. and Henikoff, S. (2020) 'Efficient low-cost chromatin profiling with CUT&Tag', *Nat Protoc* 15(10): 3264-3283.

Kim, D., Langmead, B. and Salzberg, S. L. (2015) 'HISAT: a fast spliced aligner with low memory requirements', *Nat Methods* 12(4): 357-60.

Kurita, M., Holloway, T., Garcia-Bea, A., Kozlenkov, A., Friedman, A. K., Moreno, J. L., Heshmati, M., Golden, S. A., Kennedy, P. J., Takahashi, N. et al. (2012) 'HDAC2 regulates atypical antipsychotic responses through the modulation of mGlu2 promoter activity', *Nat Neurosci* 15(9): 1245-54.

Langmead, B. and Salzberg, S. L. (2012) 'Fast gapped-read alignment with Bowtie 2', *Nat Methods* 9(4): 357-9.

Li, H., Handsaker, B., Wysoker, A., Fennell, T., Ruan, J., Homer, N., Marth, G., Abecasis, G., Durbin, R. and Genome Project Data Processing, Subgroup (2009) 'The Sequence Alignment/Map format and SAMtools', *Bioinformatics* 25(16): 2078-9.

Liao, Y., Smyth, G. K. and Shi, W. (2014) 'featureCounts: an efficient general purpose program for assigning sequence reads to genomic features', *Bioinformatics* 30(7): 923-30.

Liu, X., Wang, C., Liu, W., Li, J., Li, C., Kou, X., Chen, J., Zhao, Y., Gao, H., Wang, H. et al. (2016) 'Distinct features of H3K4me3 and H3K27me3 chromatin domains in pre-implantation embryos', *Nature* 537(7621): 558-562.

Love, M. I., Huber, W. and Anders, S. (2014) 'Moderated estimation of fold change and dispersion for RNA-seq data with DESeq2', *Genome Biol* 15(12): 550.

Lu, F., Liu, Y., Inoue, A., Suzuki, T., Zhao, K. and Zhang, Y. (2016) 'Establishing Chromatin Regulatory Landscape during Mouse Preimplantation Development', *Cell* 165(6): 1375-1388.

Luo, J., Su, F., Chen, D., Shiloh, A. and Gu, W. (2000) 'Deacetylation of p53 modulates its effect on cell growth and apoptosis', *Nature* 408(6810): 377-81.

Ma, P., Pan, H., Montgomery, R. L., Olson, E. N. and Schultz, R. M. (2012) 'Compensatory functions of histone deacetylase 1 (HDAC1) and HDAC2 regulate transcription and apoptosis during mouse oocyte development', *Proc Natl Acad Sci U S A* 109(8): E481-9.

Ma, P. and Schultz, R. M. (2008) 'Histone deacetylase 1 (HDAC1) regulates histone acetylation, development, and gene expression in preimplantation mouse embryos', *Dev Biol* 319(1): 110-20.

Ma, P. and Schultz, R. M. (2013) 'Histone deacetylase 2 (HDAC2) regulates chromosome segregation and kinetochore function via H4K16 deacetylation during oocyte maturation in mouse', *PLoS Genet* 9(3): e1003377.

Mal, A., Sturniolo, M., Schiltz, R. L., Ghosh, M. K. and Harter, M. L. (2001) 'A role for histone deacetylase HDAC1 in modulating the transcriptional activity of MyoD: inhibition of the myogenic program', *EMBO J* 20(7): 1739-53.

Matoba, S., Liu, Y., Lu, F., Iwabuchi, K. A., Shen, L., Inoue, A. and Zhang, Y. (2014) 'Embryonic development following somatic cell nuclear transfer impeded by persisting histone methylation', *Cell* 159(4): 884-95.

Nalawansha, D. A., Gomes, I. D., Wambua, M. K. and Pflum, M. K. H. (2017) 'HDAC Inhibitor-Induced Mitotic Arrest Is Mediated by Eg5/KIF11 Acetylation', *Cell Chemical Biology* 24(4): 481-+.

Quinlan, A. R. (2014) 'BEDTools: The Swiss-Army Tool for Genome Feature Analysis', *Curr Protoc Bioinformatics* 47: 11 12 1-34.

Quinlan, A. R. and Hall, I. M. (2010) 'BEDTools: a flexible suite of utilities for comparing genomic features', *Bioinformatics* 26(6): 841-2.

Ramirez, F., Dundar, F., Diehl, S., Gruning, B. A. and Manke, T. (2014) 'deepTools: a flexible platform for exploring deep-sequencing data', *Nucleic Acids Res* 42(Web Server issue): W187-91.

Santenard, A., Ziegler-Birling, C., Koch, M., Tora, L., Bannister, A. J. and Torres-Padilla, M. E. (2010) 'Heterochromatin formation in the mouse embryo requires critical residues of the histone variant H3.3', *Nat Cell Biol* 12(9): 853-62.

Schultz, R. M., Stein, P. and Svoboda, P. (2018) 'The oocyte-to-embryo transition in mouse: past, present, and future', *Biol Reprod* 99(1): 160-174.

Sheikh, B. N. and Akhtar, A. (2019) 'The many lives of KATs - detectors, integrators and modulators of the cellular environment', *Nat Rev Genet* 20(1): 7-23.

Shi, Y., Zhao, P., Dang, Y., Li, S., Luo, L., Hu, B., Wang, S., Wang, H. and Zhang, K. (2021) 'Functional roles of the chromatin remodeler SMARCA5 in mouse and bovine preimplantation embryosdagger', *Biol Reprod* 105(2): 359-370.

Skene, P. J., Henikoff, J. G. and Henikoff, S. (2018) 'Targeted in situ genome-wide profiling with high efficiency for low cell numbers', *Nat Protoc* 13(5): 1006-1019.

Trapnell, C., Roberts, A., Goff, L., Pertea, G., Kim, D., Kelley, D. R., Pimentel, H., Salzberg, S. L., Rinn, J. L. and Pachter, L. (2012) 'Differential gene and transcript expression analysis of RNA-seq experiments with TopHat and Cufflinks', *Nat Protoc* 7(3): 562-78.

Vastenhouw, N. L., Cao, W. X. and Lipshitz, H. D. (2019) 'The maternal-to-zygotic transition revisited', *Development* 146(11).

Wang, Chenfei, Chen, Chuan, Liu, Xiaoyu, Li, Chong, Wu, Qiu, Chen, Xiaolan, Yang, Lingyue, Kou, Xiaochen, Zhao, Yanhong, Wang, Hong et al. (2022) 'Dynamic nucleosome organization after fertilization reveals regulatory factors for mouse zygotic genome activation': 2022.03.03.482916.

Wang, H., Wang, L., Wang, Z., Dang, Y., Shi, Y., Zhao, P. and Zhang, K. (2020) 'The nucleolar protein NOP2 is required for nucleolar maturation and ribosome biogenesis during preimplantation development in mammals', *FASEB J* 34(2): 2715-2729.

Wu, J., Huang, B., Chen, H., Yin, Q., Liu, Y., Xiang, Y., Zhang, B., Liu, B., Wang, Q., Xia, W. et al. (2016) 'The landscape of accessible chromatin in mammalian preimplantation embryos', *Nature* 534(7609): 652-7.

Xia, W., Xu, J., Yu, G., Yao, G., Xu, K., Ma, X., Zhang, N., Liu, B., Li, T., Lin, Z. et al. (2019) 'Resetting histone modifications during human parental-to-zygotic transition', *Science* 365(6451): 353-360.

Xu, Q. and Xie, W. (2018) 'Epigenome in Early Mammalian Development: Inheritance, Reprogramming and Establishment', *Trends Cell Biol* 28(3): 237-253.

Xu, R., Li, C., Liu, X. and Gao, S. (2021a) 'Insights into epigenetic patterns in mammalian early embryos', *Protein & Cell* 12(1): 7-28.

Xu, R. M., Li, C., Liu, X. Y. and Gao, S. R. (2021b) 'Insights into epigenetic patterns in mammalian early embryos', *Protein & Cell* 12(1): 7-28.

Yang, G., Zhang, L., Liu, W., Qiao, Z., Shen, S., Zhu, Q., Gao, R., Wang, M., Wang, M., Li, C. et al. (2021) 'Dux-Mediated Corrections of Aberrant H3K9ac during 2-Cell Genome Activation Optimize Efficiency of Somatic Cell Nuclear Transfer', *Cell Stem Cell* 28(1): 150-163 e5.

Yu, G., Wang, L. G. and He, Q. Y. (2015) 'ChIPseeker: an R/Bioconductor package for ChIP peak annotation, comparison and visualization', *Bioinformatics* 31(14): 2382-3.

Zeng, F. and Schultz, R. M. (2005) 'RNA transcript profiling during zygotic gene activation in the preimplantation mouse embryo', *Dev Biol* 283(1): 40-57.

Zhang, B., Wu, X., Zhang, W., Shen, W., Sun, Q., Liu, K., Zhang, Y., Wang, Q., Li, Y., Meng, A. et al. (2018) 'Widespread Enhancer Dememorization and Promoter Priming during Parental-to-Zygotic Transition', *Mol Cell* 72(4): 673-686 e6.

Zhang, B., Zheng, H., Huang, B., Li, W., Xiang, Y., Peng, X., Ming, J., Wu, X., Zhang, Y., Xu, Q. et al. (2016) 'Allelic reprogramming of the histone modification H3K4me3 in early mammalian development', *Nature* 537(7621): 553-557.

Zhang, L., Hou, X., Ma, R., Moley, K., Schedl, T. and Wang, Q. (2014) 'Sirt2 functions in spindle organization and chromosome alignment in mouse oocyte meiosis', *FASEB J* 28(3): 1435-45.

Zhang, Y., Liu, T., Meyer, C. A., Eeckhoute, J., Johnson, D. S., Bernstein, B. E., Nusbaum, C., Myers, R. M., Brown, M., Li, W. et al. (2008) 'Model-based analysis of ChIP-Seq (MACS)', *Genome Biol* 9(9): R137.

Zhao, P., Wang, H., Wang, H., Dang, Y., Luo, L., Li, S., Shi, Y., Wang, L., Wang, S., Mager, J. et al. (2020) 'Essential roles of HDAC1 and 2 in lineage development and genome-wide DNA methylation during mouse preimplantation development', *Epigenetics* 15(4): 369-385.

Zhou, N., Cao, Z., Wu, R., Liu, X., Tao, J., Chen, Z., Song, D., Han, F., Li, Y., Fang, F. et al. (2014) 'Dynamic changes of histone H3 lysine 27 acetylation in pre-implantational pig embryos derived from somatic cell nuclear transfer', *Anim Reprod Sci* 148(3-4): 153-63.

Figures

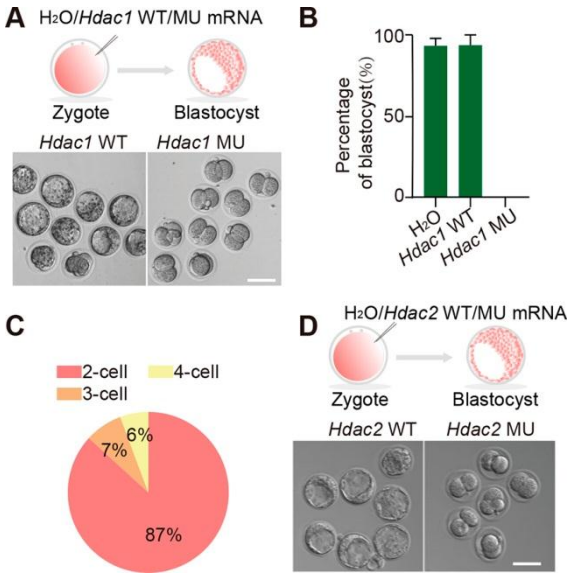

Fig. 1 HDAC1/2 is essential for ZGA in mouse and bovine embryos. A, Experimental scheme (top) and representative images (bottom) of embryos injected with *Hdac1* wild type mRNA and *Hdac1* mutant mRNA on day 4.5 after fertilization, scale bar, 25 μm. **B,** Percentage of blastocysts at day 4.5 after fertilization in three groups. Data shown as Means ± SEM (n = 3; 9-15 embryos per group per replicate). **C,** Distribution of cleavage embryos found in embryos injected with *Hdac1* mutant mRNA at day 4.5 after fertilization. **D,** Experimental scheme (top) and representative images (bottom) of embryos injected with *Hdac2* wild type mRNA and *Hdac2* mutant mRNA on day 4.5 after fertilization, scale bar, 25 μm.

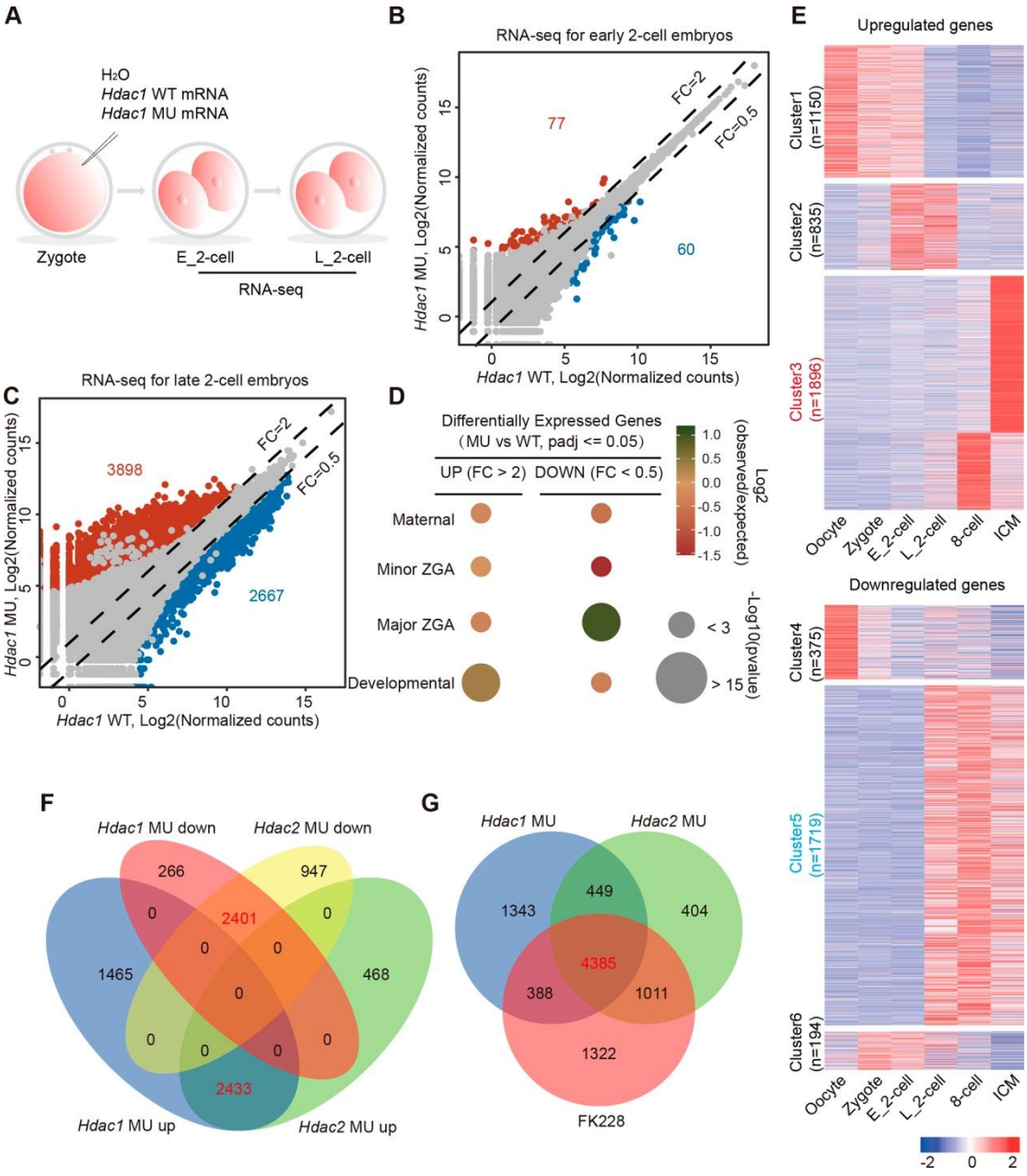

Fig. 2 HDAC1 mutation results in aberrant gene expression pattern during ZGA. **A,** Experimental scheme of RNA-seq. **B and C,** Scatter plots showing global gene expression in embryos injected with *Hdac1* WT mRNA or *Hdac1* MU mRNA at early 2-cell stage (B) and late 2-cell stage (C). Two RNA-seq replicates are generated for differential expression analysis, and the read counts are normalized by DESeq2. Dash lines indicate the threshold of fold change (MU/WT), and grey dots refer to genes with *Padj* > 0.05, while dots in red and blue refer to genes with *Padj* <= 0.05. Numbers of up- and down- regulated genes are indicated in the figures. **D,** Overlap of

all differentially expressed genes with different gene categories. The gene categories are generated with *k-means* clustering of RNA-seq data(Wu et al., 2016) for mouse oocytes and zygote, early 2-cell, late 2-cell, 8-cell embryos and ICM. The color of bubbles refers to $\log_2$ ratio of number of observed genes in the gene set relative to randomly expected frequencies, and the size of bubbles shows $-\log_{10}$ of Fisher-exact test *P* value. **E,** Heatmaps showing relative expression of up- (top, *Hdac1* MU/WT FC > 2 and *Padj* <= 0.05) and down-regulated (bottom, *Hdac1* MU/WT FC < 0.5 and *Padj* <= 0.05) genes during wild type mouse preimplantation development. The differential expressed genes are classified to 6 clusters by *k-means* clustering. RNA-seq data for wild type embryos was obtained from the published work(Wu et al., 2016)**. F,** Venn diagram showing overlap of up- and down-regulated genes induced by overexpression of *Hdac1* and *Hdac2* MU mRNA. Note that size of the circles doesn't reflect the number of genes. **G,** Overlap of all differentially expressed genes induced by overexpression of *Hdac1* or *Hdac2* MU mRNA and treatment of FK228. Size of the circles doesn't equal to the number of genes.

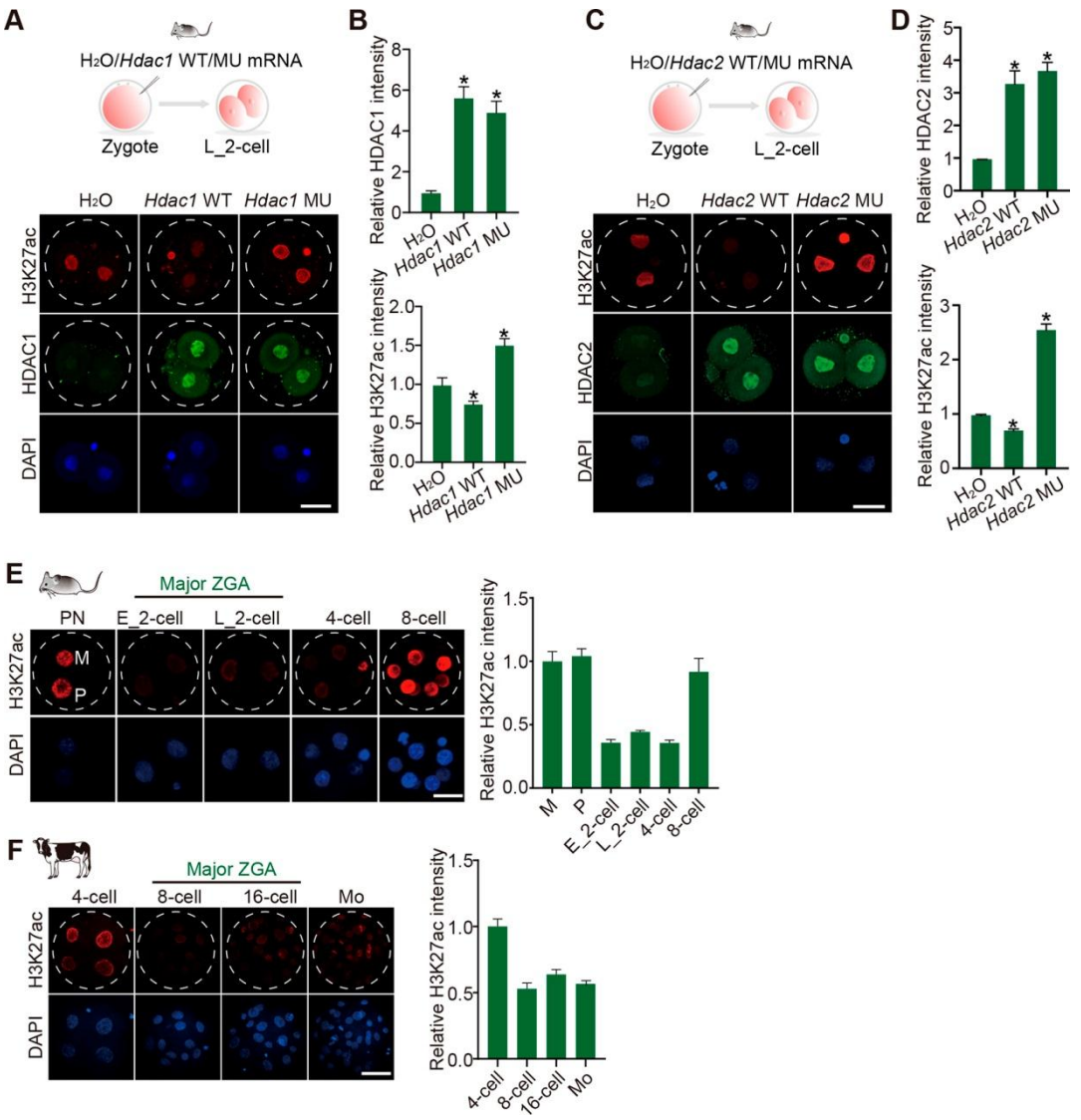

Fig. 3 The lysine deacetylase activity of HDAC1/2 is required for reprogramming of histone acetylation during ZGA. A, Experimental scheme (top) and immunofluorescence staining (bottom) of HDAC1 and H3K27ac in late 2-cell embryos, scale bar: 25 μm. **B,** HDAC1 (top) or H3K27ac (bottom) intensity relative to embryos injected with H_2O. Data shown as Means ± SEM (n = 3; 3-10 embryos per group per replicate, *P < 0.05 (*Hdac1* WT or MU vs H_2O)). **C,** Experimental scheme (top) and immunofluorescence staining (bottom) of HDAC2 and H3K27ac in mouse late 2-cell embryos, scale bar, 25 μm, **D,** HDAC2 (top) and H3K27ac (bottom) intensity relative to embryos injected with H_2O. Data shown as Means ± SEM (n = 3; 3-7 embryos per group per replicate, *P < 0.05 (*Hdac2* MU or WT vs H_2O)). **E,** Immunofluorescence staining of H3K27ac in mouse pronuclear stage (PN) zygote,

early 2-cell (E_2-cell), late 2-cell (L_2-cell), 4-cell and 8-cell embryos. Left: representative images; M, maternal pronucleus, P, paternal pronucleus; scale bar, 25 μm. right: H3K27ac intensity relative to maternal pronucleus. Data shown as Means ± SEM (n = 3; 3-10 embryos per group per replicate). **F,** Immunofluorescence staining of H3K27ac in bovine 4-, 8-, 16-cell embryos and morulae. Left: representative images; scale bar, 50 μm. right: H3K27ac intensity relative to 4-cell embryos. Data shown as Means ± SEM (n = 3; 3-7 embryos per group per replicate).

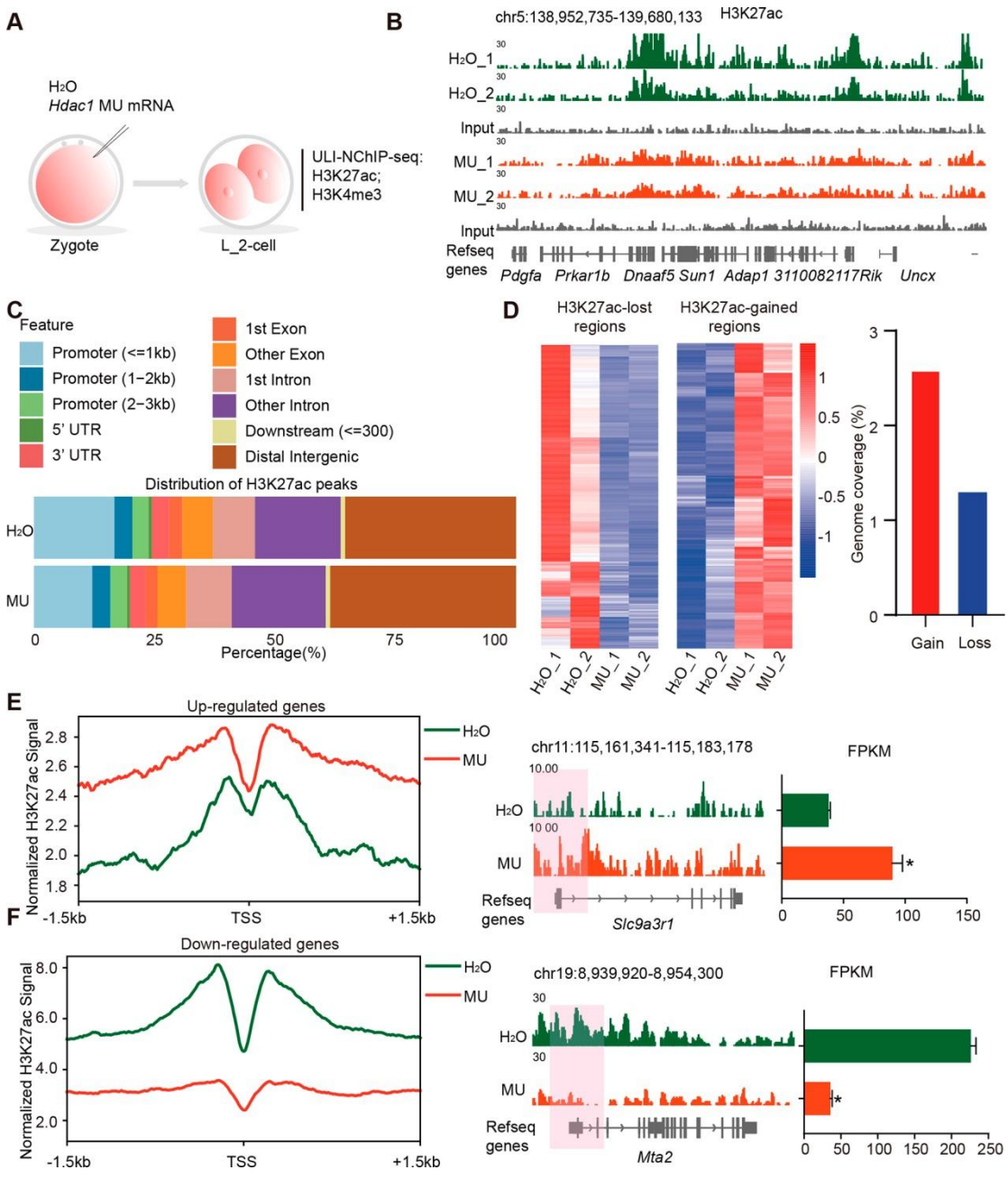

Fig. 4 HDAC1 mutation results in aberrant distribution of H3K27ac in early embryos. A, Experimental scheme for ULI-ChIP-seq. **B,** IGV browser snapshots showing H3K27ac signals in two biological replicates of embryos injected with H_2O and *Hdac1* MU mRNA respectively. **C,** Genomic annotation of H3K27ac peaks in the two groups. **D,** Heatmaps showing z-score normalized RPKM of H3K27ac-lost and -gained regions. Bar plots display the genomic coverage for those regions. Identification of H3K27ac-lost and -gained regions is described in the Methods section. **E and F,** The left panel showing profile of H3K27ac signal at promoters of

all up-regulated genes (*Hdac1* MU/WT FC > 2 and *Padj* <= 0.05) (E) and down-regulated genes (*Hdac1* MU/WT FC < 0.5 and *Padj* <= 0.05) (F). H3K27ac signal is normalized to RPKM by DeepTools. The right panel showing IGV browser snapshot of an up-regulated gene (E) and a down-regulated gene (F). The corresponding FPKM in RNA-seq data is showed in bar plots. **Padj* < 0.05.

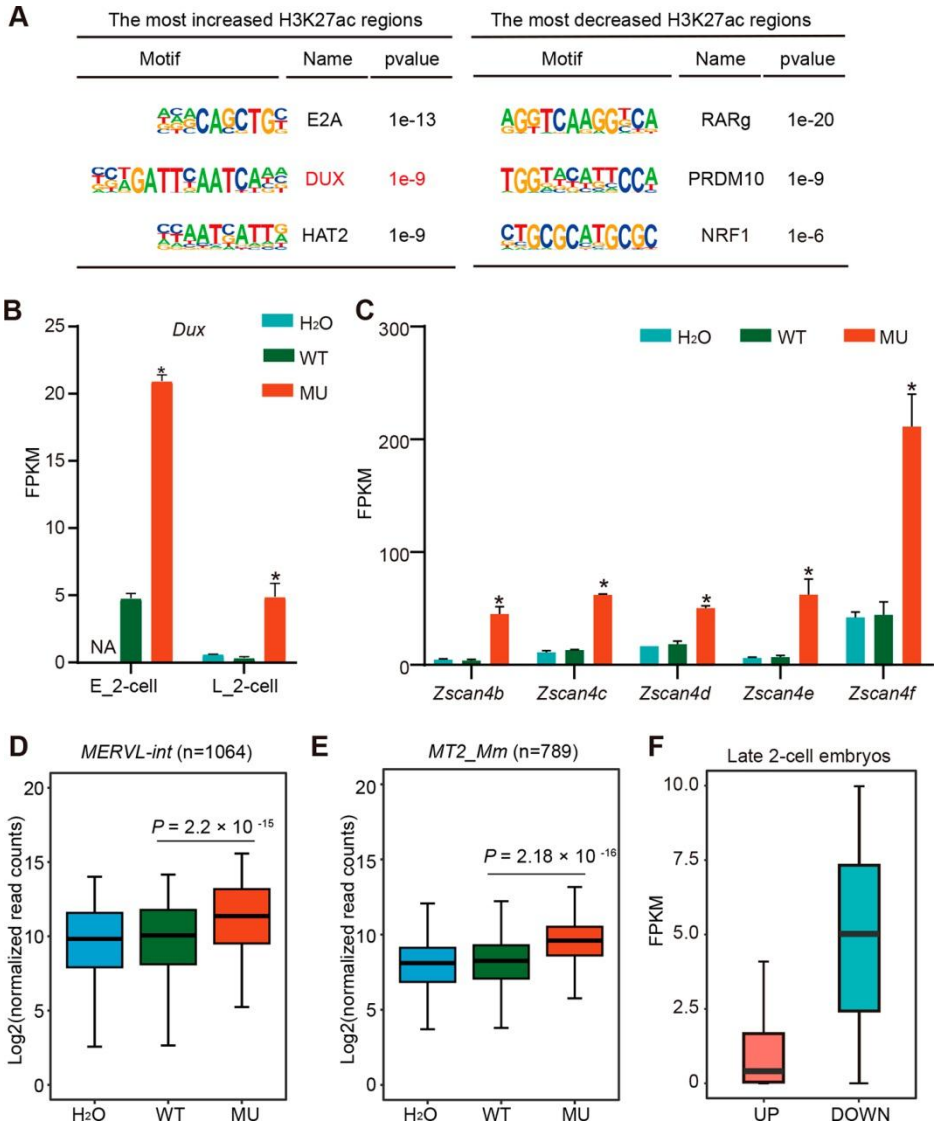

Fig. 5 DUX is up-regulated upon HDAC1 mutation. A, Representative motifs enriched at the most H3K27ac-increased and -decreased regions (with *p* value) are listed. Identification for the most H3K27ac-increased and -decreased regions is descripted in the Method section. **B,** Relative expression of *Dux* (also known as *Duxf3*) in early and late 2-cell embryos. **Padj* < 0.05 (MU vs WT). NA: not available. **C,** Relative expression of *Zscan4s* in late 2-cell embryos. **Padj* < 0.05 (MU vs WT). **D and E,** Box plots showing expression of *MERVL-int* (n=1064) and *MT2_Mm* (n=789) in late 2-cell embryos. Read counts are normalized by DESeq2. *P* values are calculated by Wilcoxon rank sum test. **F,** Box plots showing average expression levels of up-regulated (*Hdac1* MU/WT FC > 2 and *Padj* <= 0.05) and down-regulated (*Hdac1* MU/WT FC < 0.5 and *Padj* <= 0.05) genes in H_2O injection embryos at late 2-cell stage.

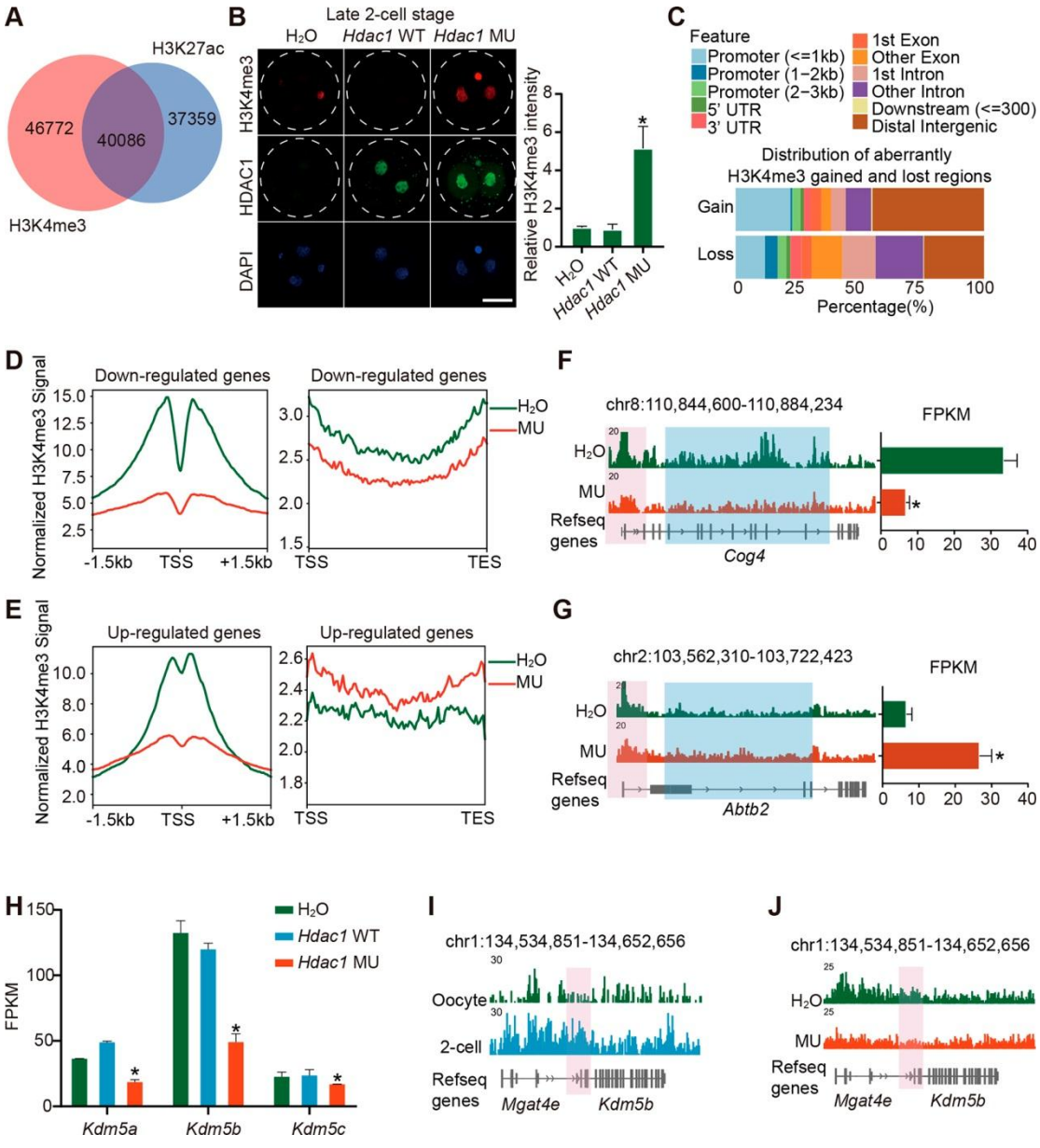

Fig. 6 HDAC1 mutation inhibits the removal of H3K4me3 during mouse ZGA. A, Venn diagram showing the overlap of H3K27ac peaks and H3K4me3 peaks in mouse late 2-cell embryos of H_2O injection group. **B,** Immunofluorescence staining of H3K4me3 and HDAC1 at late 2-cell stage in three groups. Left: representative images, scale bar, 25 μm, right: H3K4me3 intensity relative to H_2O-injected embryos. Data shown as Means ± SEM (n = 3; 3-10 embryos per group per replicate, *$P<0.05$ (MU vs WT or H_2O)). **C,** Genomic annotation of H3K4me3-gained and -lost regions. Identification of H3K4me3-lost and -gained regions is described in the Methods section. **D and E,** The left panel shows profiles of H3K4me3 signal at promoters of

all down-regulated genes (*Hdac1* MU/WT FC < 0.5 and *Padj* <= 0.05) (D) and up-regulated genes (*Hdac1* MU/WT FC > 2 and *Padj* <= 0.05) (E). The right panel shows profiles of H3K4me3 signal in gene body regions of all down-regulated (D) and up-regulated (E) genes. H3K4me3 signal is normalized to RPKM by DeepTools. **F and G,** Browser snapshots showing H3K4me3 at down-regulated genes (F) and up-regulated genes (G). The relative expression is showed in bar plots. **Padj* < 0.05. **H,** Relative expression of *Kdm5a, Kdm5b, Kdm5c* in late 2-cell embryos. **Padj* < 0.05. **I,** Browser snapshots showing H3K27ac at *Kdm5b* in wildtype oocytes and 2-cell embryos. **J,** Browser snapshots showing H3K27ac at *Kdm5b* in late 2-cell embryos.

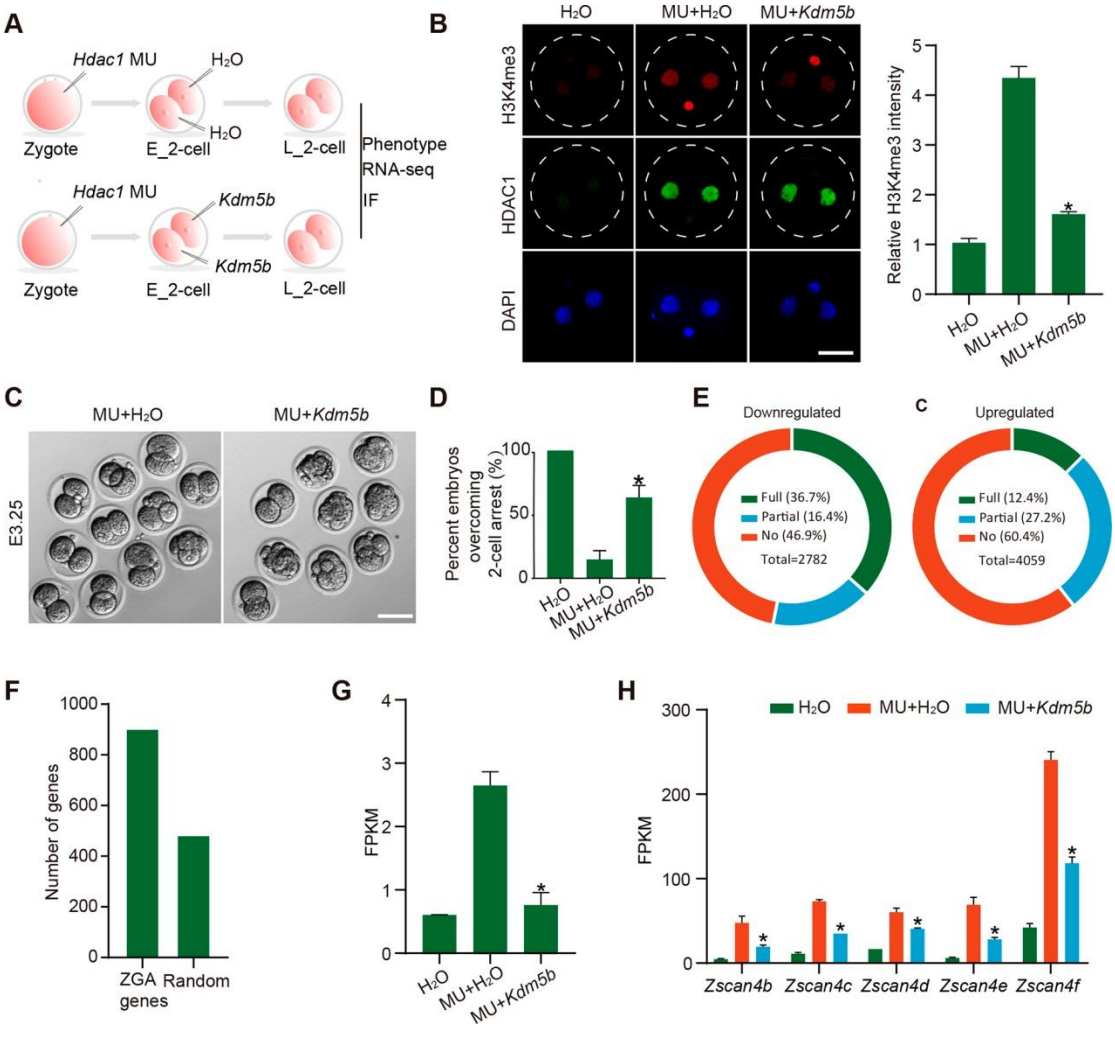

Fig. 7 KDM5B is a key mediator of the HDCA1 MU phenotype. A, Experimental scheme showing overexpression of exogenous *Kdm5b* in early embryos. **B,** Immunofluorescence staining of H3K4me3 and HDAC1 at late 2-cell stage. Left: representative images, scale bar, 25 µm, right: H3K4me3 intensity relative to embryos injected with *Hdac1* MU mRNA and H_2O. Data shown as Means ± SEM (n=3; 3-10 embryos per group per replicate, $*P < 0.05$ (H1MU+*Kdm5b* vs H1MU+H_2O)). **C,** Developmental progression of embryos in the two groups at day 3.25 after fertilization. **D,** The ratio of embryos developing beyond 2-cell stage at day 3.25 after fertilization. Data shown as Means ± SEM (n = 3; 9-15 embryos per group per replicate, $*P < 0.05$ (H1MU+*Kdm5b* vs H1MU+H_2O)). **E,** Donut chart of down-regulated genes (H1MU/ H_2O, left) and up-regulated genes (H1MU/H_2O , right) based on their extent of rescue in H1MU+*Kdm5b* mRNA injection embryos. Full

rescue genes refers to those downregulated or upregulated genes that are not differentially expressed in H1MU+Kdm5 group (Downregulated genes: Padj>0.05 or log2FoldChange (H1MU+Kdm5b/H2O-injected)>-1; Upregulated genes: Padj>0.05 or log2FoldChange (H1MU+Kdm5b/ H2O-injected)<1). Partial rescue genes refers to those downregulated genes that still downregulated and those upregulated genes that still upregulated in H1MU+Kdm5b but partially rescued compared to H1MU group (Downregulated genes: log2FoldChange(H1MU+Kdm5b/H1MU+H2O)>0.5; Upregulated genes: log2FoldChange (H1MU+Kdm5b/H1MU+H2O)<-0.5). The rest of downregulated and upregulated genes are "no rescue" genes. **F,** Number of up-regulated (H1MU+*Kdm5b* vs MU+H_2O) major ZGA genes and the number expected by chance, Fisher exact test *P* value < 10^{-10}. **G,** Relative expression of *Dux* (also known as *Duxf3*). **Padj* < 0.05 (H1MU+*Kdm5b* vs H1MU+H_2O). **H,** Relative expression of *Zscan4s*. **Padj* < 0.05 (H1MU+*Kdm5b* vs H1MU+H_2O).

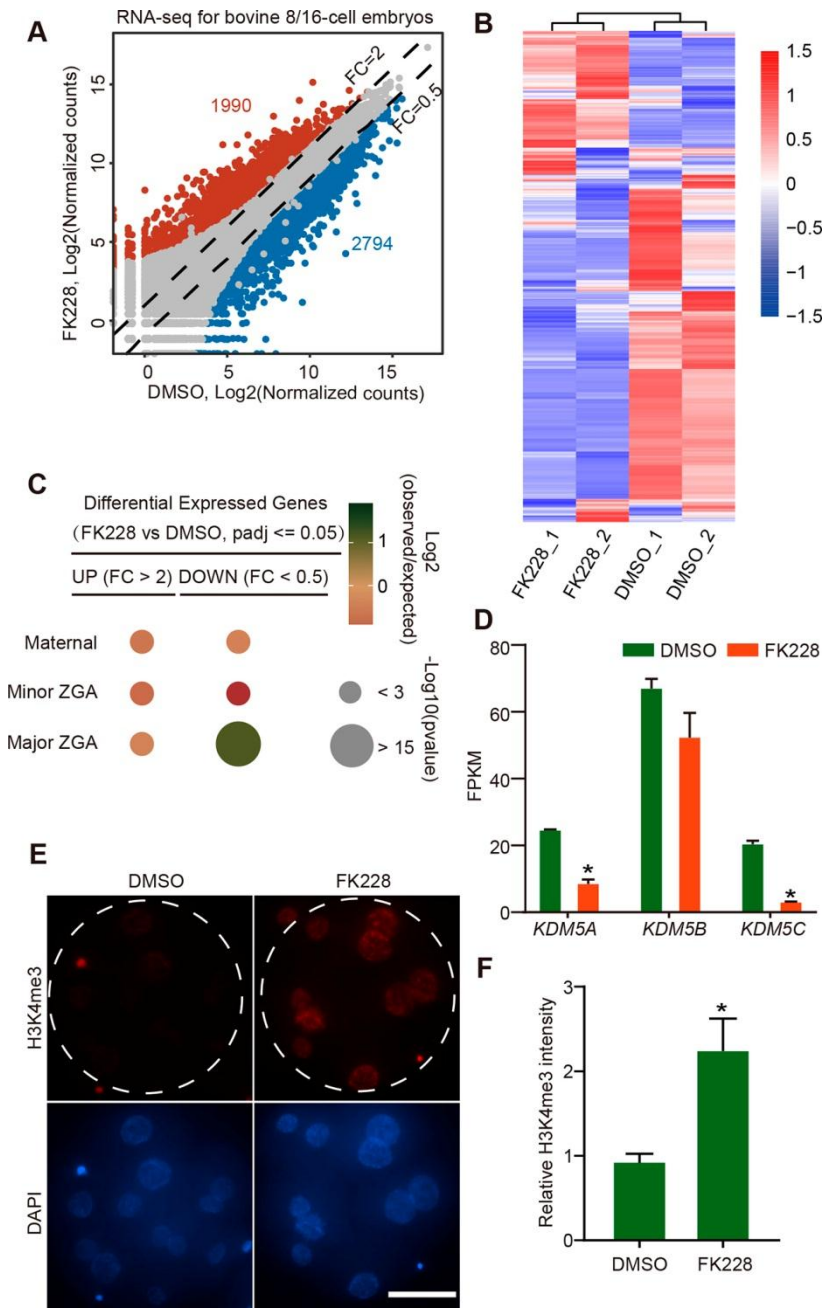

Fig. 8 Function of HDAC1/2 on major ZGA is conserved in bovine embryos. A, Scatter plots showing gene expression level in embryos treated with DMSO (negative control) and FK228 in bovine 8/16-cell embryos. Two RNA-seq replicates are generated for differential expression analysis, and the read counts are normalized by DESeq2. Dash lines indicate the threshold of fold change (FK228/DMSO), and grey dots refer to genes with *Padj* > 0.05, while dots in red and blue refer to genes with *Padj* <= 0.05. Numbers of up- and down- regulated genes are also indicated in the

figures. **B,** Relative expression of all bovine major ZGA genes in DMSO and FK228 treated embryos. **C,** Overlap of all differentially expressed genes with different gene categories. The gene categories are generated with *k-means* clustering of RNA-seq data(Graf et al., 2014) for bovine MII oocytes and 4-cell, 8-cell, 16-cell embryos. The color of bubbles refers to $\log_2$ ratio of the number of observed genes in the gene set to randomly expected frequencies, and the size of bubbles shows $-\log_{10}$ of Fisher-exact test *P* value. **D,** Relative expression of *KDM5A*, *KDM5B*, *KDM5C* in DMSO and FK228 treated embryos. **Padj* < 0.05. **E and F,** Immunofluorescence staining of H3K4me3 in bovine 8/16-cell embryos. E, representative images, scale bar, 50 μm, F, H3K4me3 intensity relative to DMSO-treated embryos. Data shown as Means ± SEM (n=3; 3-7 embryos per group per replicate, **P* < *0.05*).

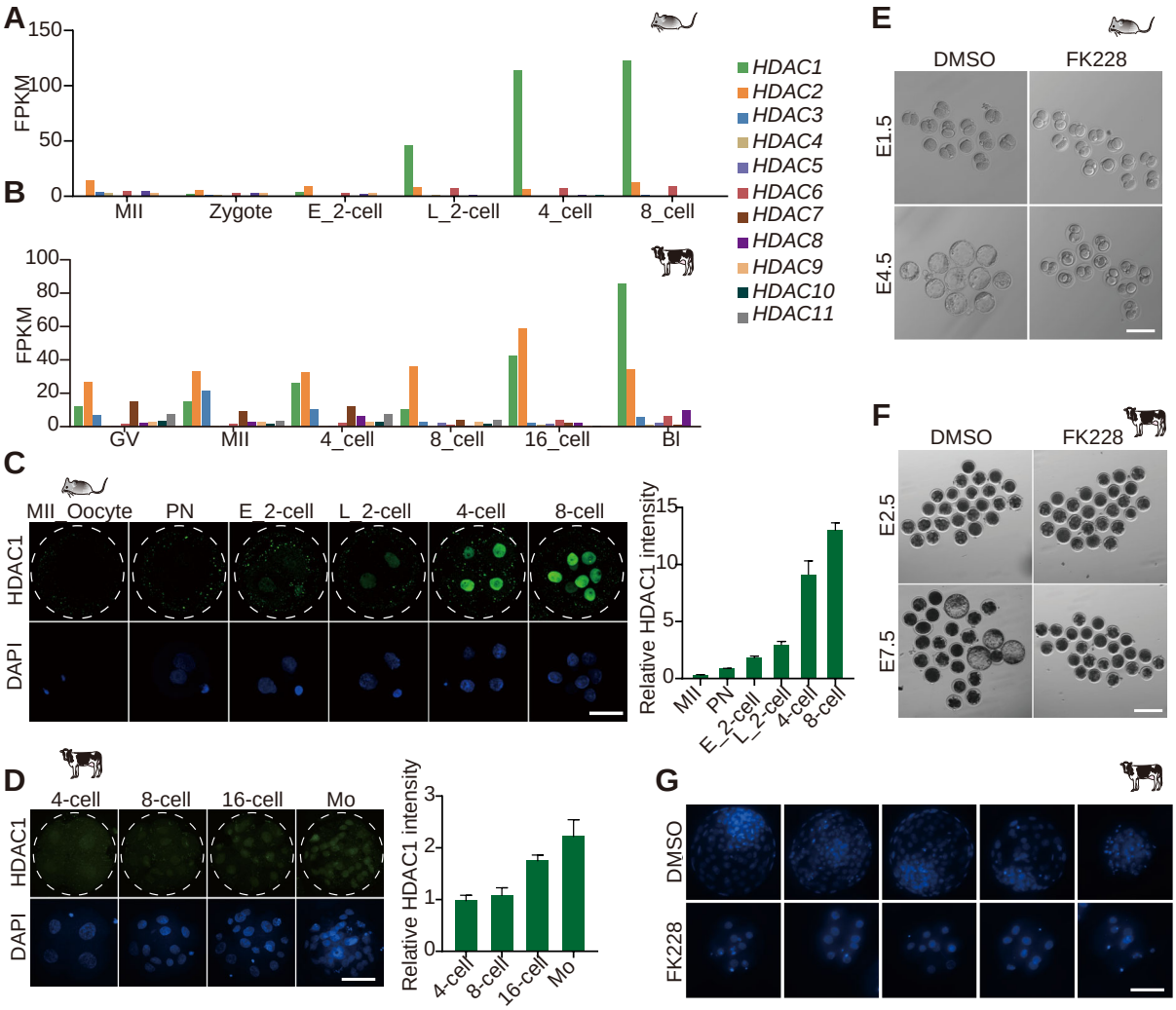

Fig. S1. HDAC1/2 is essential for ZGA in mouse and bovine embryos. A and B, Relative expression of *Hdacs* in mouse (A) and bovine (B) oocytes and preimplantation embryos. **C,** Immunofluorescence staining of HDAC1 for mouse oocytes and preimplantation embryos. Left: representative images, scale bar, 25 μm, right: HDAC1 intensity relative to MII oocytes. Data shown as Means ± s.e.m. (n = 3; 3-7 embryos per group per replicate). **D,** Immunofluorescence staining of HDAC1 for bovine preimplantation embryos. Left: representative images, scale bar, 50 μm, right: HDAC1 intensity relative to 4-cell embryos. Data shown as Means ± s.e.m. (n=3; 3-7 embryos per group per replicate). **E,** Representative images in bright field at day 1.5 and day 4.5 after fertilization of mouse embryos treated with DMSO or FK228. **F,** Representative images in bright field at day 2.5 and day 7.5 after fertilization of bovine embryos treated with DMSO or FK228. **G,** DNA staining with DAPI at day 7.5 after fertilization for bovine embryos treated with DMSO or FK228, scale bar, 50 μm.

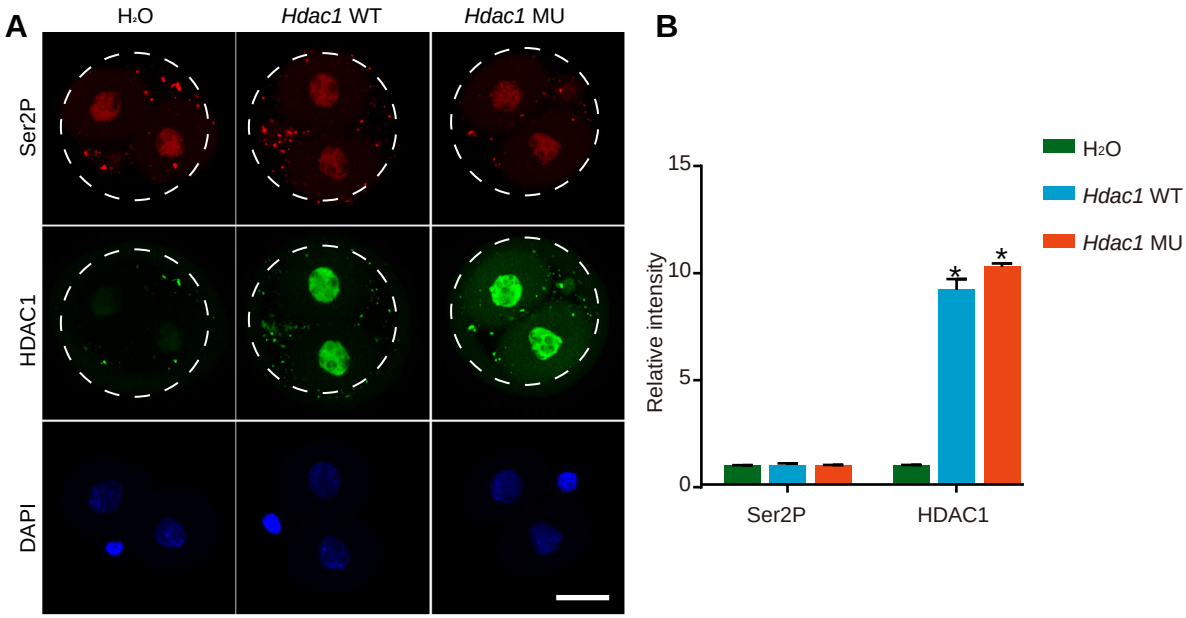

Fig. S2. Global transcriptional activity of mouse embryos. A, Representative images of HDAC1 and Phospho-RNA pol II C-terminal domain (Ser2P) immunofluorescence staining in mouse late 2-cell embryos, scale bar, 25 μm, **B,** HDAC1 and Ser2P intensity relative to H_2O-injected embryos. Data shown as Means ± s.e.m. (n = 3; 3-7 embryos per group per replicate, *$P < 0.05$ (MU or WT vs H_2O))

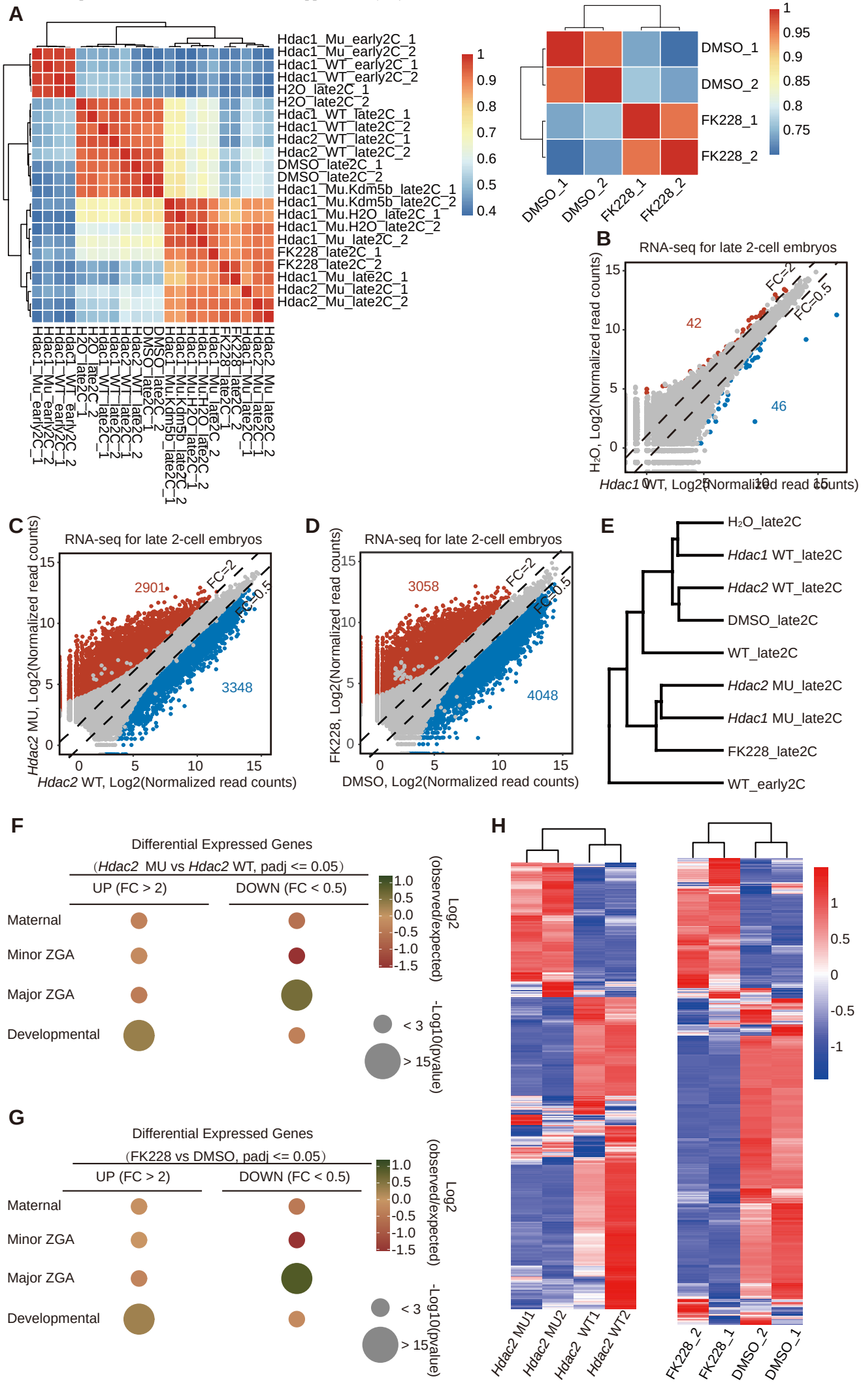
A
Hdac1_Mu_early2C_1
Hdac1_Mu_early2C_2
Hdac1_WT_early2C_1
Hdac1_WT_early2C_2
H2O_late2C_1
H2O_late2C_2
Hdac1_WT_late2C_1
Hdac1_WT_late2C_2
Hdac2_WT_late2C_1
Hdac2_WT_late2C_2
DMSO_late2C_1
DMSO_late2C_2
Hdac1_Mu.Kdm5b_late2C_1
Hdac1_Mu.Kdm5b_late2C_2
Hdac1_Mu.H2O_late2C_1
Hdac1_Mu.H2O_late2C_2
Hdac1_Mu_late2C_2
FK228_late2C_1
FK228_late2C_2
Hdac1_Mu_late2C_1
Hdac2_Mu_late2C_1
Hdac2_Mu_late2C_2
1
0.9
0.8
0.7
0.6
0.5
0.4
DMSO_1
DMSO_2
FK228_1
FK228_2
1
0.95
0.9
0.85
0.8
0.75
B
RNA-seq for late 2-cell embryos
H2O, Log2(Normalized read counts)
Hdac1 WT, Log2(Normalized read counts)
FC=2
FC=0.5
42
46
C
RNA-seq for late 2-cell embryos
Hdac2 MU, Log2(Normalized read counts)
Hdac2 WT, Log2(Normalized read counts)
2901
3348
D
RNA-seq for late 2-cell embryos
FK228, Log2(Normalized read counts)
DMSO, Log2(Normalized read counts)
3058
4048
E
H2O_late2C
Hdac1 WT_late2C
Hdac2 WT_late2C
DMSO_late2C
WT_late2C
Hdac2 MU_late2C
Hdac1 MU_late2C
FK228_late2C
WT_early2C
F
Differential Expressed Genes
(Hdac2 MU vs Hdac2 WT, padj <= 0.05)
UP (FC > 2)
DOWN (FC < 0.5)
Maternal
Minor ZGA
Major ZGA
Developmental
Log2 (observed/expected)
-Log10(pvalue)
< 3
> 15
G
Differential Expressed Genes
(FK228 vs DMSO, padj <= 0.05)
UP (FC > 2)
DOWN (FC < 0.5)
Maternal
Minor ZGA
Major ZGA
Developmental
Log2 (observed/expected)
-Log10(pvalue)
< 3
> 15
H
Hdac2 MU1
Hdac2 MU2
Hdac2 WT1
Hdac2 WT2
FK228_2
FK228_1
DMSO_2
DMSO_1

Fig. S3. Repression of HDAC1/2 dysregulates gene expression during mouse ZGA. A, Heatmaps showing spearman correlation coefficient of two biological replicates for mouse (left) and cattle (right) RNA-seq in this study. **B-D,** Scatter plots showing expression levels of genes in late 2-cell mouse embryos injected with *Hdac1* WT mRNA or H_2O (B) and injected with *Hdac2* WT mRNA or *Hdac2* mutant mRNA (C) and treated with DMSO or FK228 (D). Two RNA-seq replicates are generated for differential expression analysis, and the read counts are normalized by DESeq2. Dash lines indicate the threshold of fold change, and grey dots refer to genes with *Padj* > 0.05, while dots in red and blue refer to genes with *Padj* <= 0.05. Numbers of up- and down- regulated genes are also indicated in the figures. **E,** Hierarchical clustering of mouse late 2-cell embryos in different groups and wildtype embryos (WT_late2C, WT_early2C(Wu et al., 2016)) based on the FPKM in RNA-seq data. **F and G,** Overlap of all differentially expressed genes in late 2-cell embryos (F, *Hdac2* MU vs *Hdac2* WT, G, FK228 vs DMSO) with different gene sets. The gene sets are generated with *k-means* clustering of RNA-seq data(Wu et al., 2016) for mouse oocytes and zygotes, early 2-cell, late 2-cell, 8-cell embryos and ICM. The color of bubbles refers to $\log_2$ ratio of number of observed genes in the gene set to randomly expected frequencies, and the size of bubbles shows $-\log_{10}$ of Fisher exact test *p* value. **H,** Heatmaps showing expression of all major ZGA genes at late 2-cell stage.

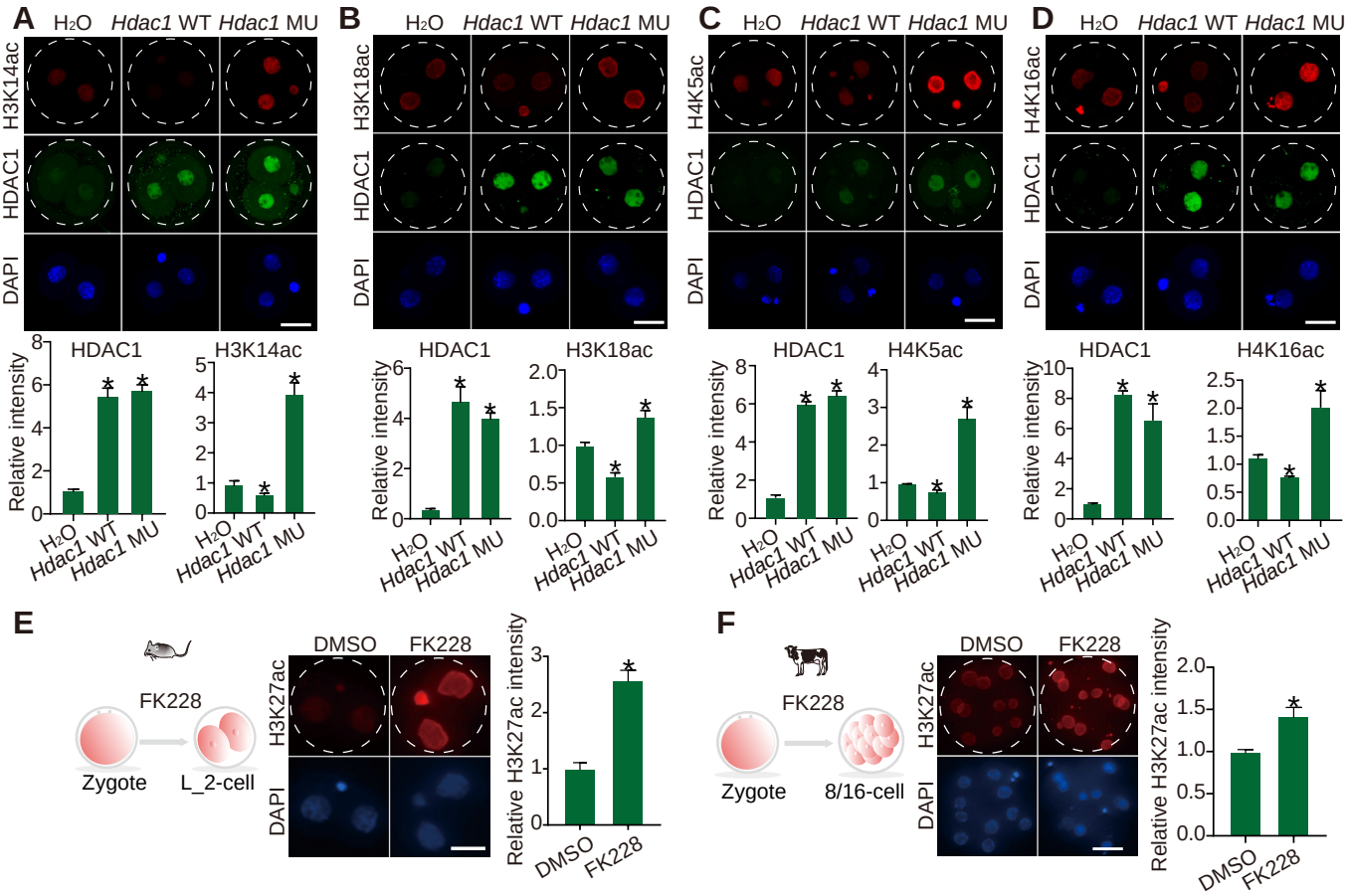

Fig. S4. The histone deacetylase activity of HDAC1/2 is required for reprogramming of histone acetylation during ZGA. A, Immunofluorescence staining (top) of HDAC1 and H3K14ac in late 2-cell embryos, scale bar: 25 μm. HDAC1 and H3K14ac (bottom) intensity relative to embryos injected with H_2O. Data shown as Means ± s.e.m. (n = 3; 3-10 embryos per group per replicate, $*P < 0.05$ (*Hdac1* WT or MU vs H_2O)). **B,** Immunofluorescence staining (top) of HDAC1 and H3K18ac in late 2-cell embryos, scale bar: 25 μm. HDAC1 and H3K18ac (bottom) intensity relative to embryos injected with H_2O. Data shown as Means ± s.e.m. (n = 3; 3-10 embryos per group per replicate, $*P < 0.05$ (*Hdac1* WT or MU vs H_2O)). **C,** Immunofluorescence staining (top) of HDAC1 and H4K5ac in late 2-cell embryos, scale bar: 25 μm. HDAC1 and H4K5ac (bottom) intensity relative to embryos injected with H_2O. Data shown as Means ± s.e.m. (n = 3; 3-10 embryos per group per replicate, $*P < 0.05$ (*Hdac1* WT or MU vs H_2O)). **D,** Immunofluorescence staining (top) of HDAC1 and H4K16ac in late 2-cell embryos, scale bar: 25 μm. HDAC1 and H4K16ac (bottom) intensity relative to embryos injected with H_2O. Data shown as Means ± s.e.m. (n = 3; 3-10 embryos per group per replicate, $*P < 0.05$ (*Hdac1* WT or MU vs H_2O)). **E,** Experimental scheme (left) showing H3K27ac immunofluorescence staining at mouse late 2-cell stage (mid), scale bar, 25 μm, H3K27ac intensity relative to DMSO-treated embryos is showed in the right panel. **F,** Experimental scheme (left) showing H3K27ac immunofluorescence staining (mid) at bovine 8/16-cell stage, scale bar, 50 μm, H3K27ac intensity relative to DMSO-treated embryos is showed in the right panel.

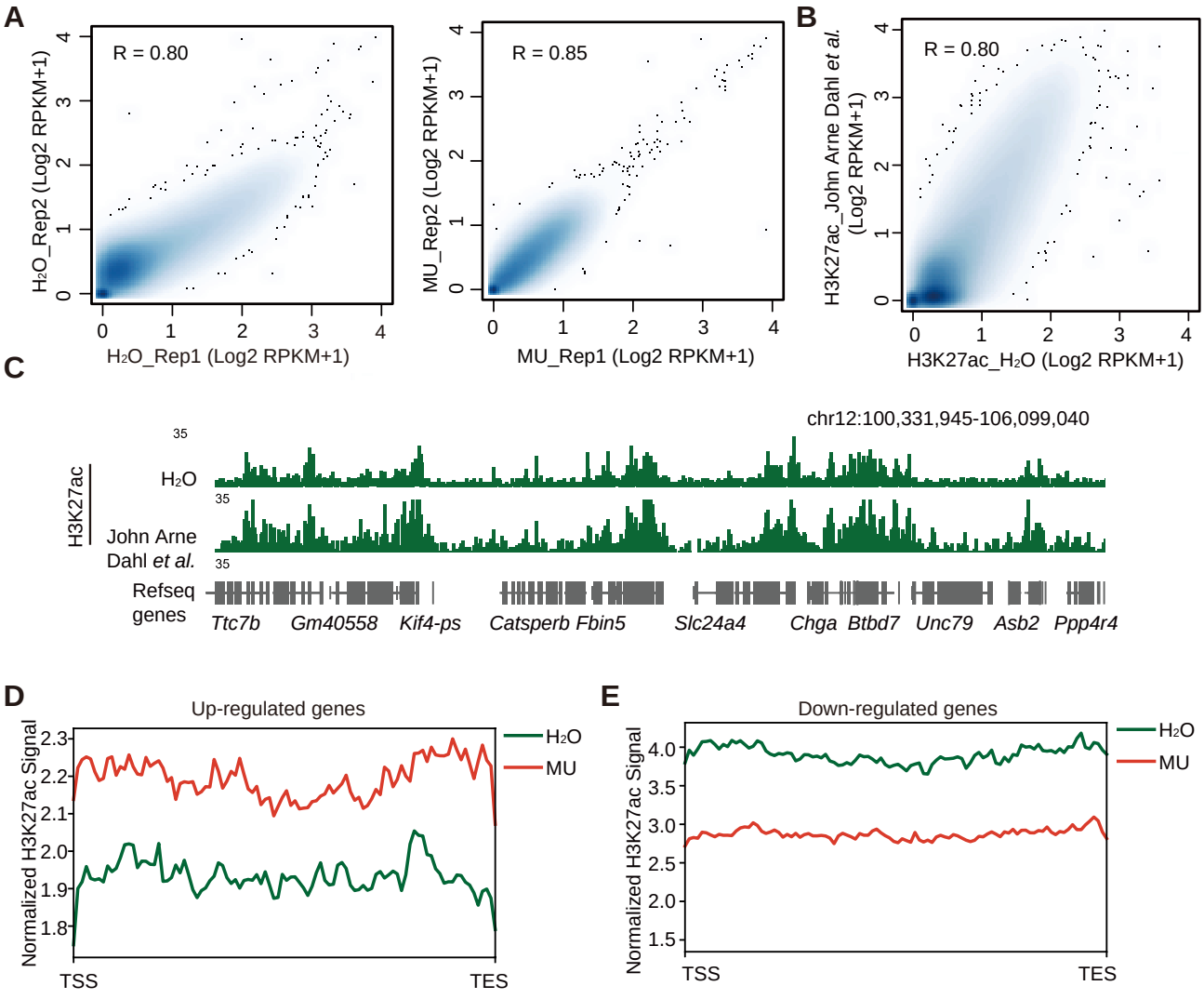

Fig. S5. HDAC1 regulates the distribution of H3K27ac during mouse ZGA. A, Scatter plots showing the H3K27ac signal (RPKM for 2-kb bin across the genome) between two biological replicates. **B,** Scatter plots showing the H3K27ac signal (RPKM for 2-kb bin across the genome) in late 2-cell embryos between data sets of this study and John Arne Dahl *et al*., R refers to Pearson correlation coefficient. **C,** Browser snapshots of H3K27ac in late 2-cell embryos injected with H_2O and published ChIP-seq data. **D and E,** H3K27ac signal in gene body regions of up-regulated (*Hdac1* MU/WT, D) and down-regulated (*Hdac1* MU/WT, E) genes.

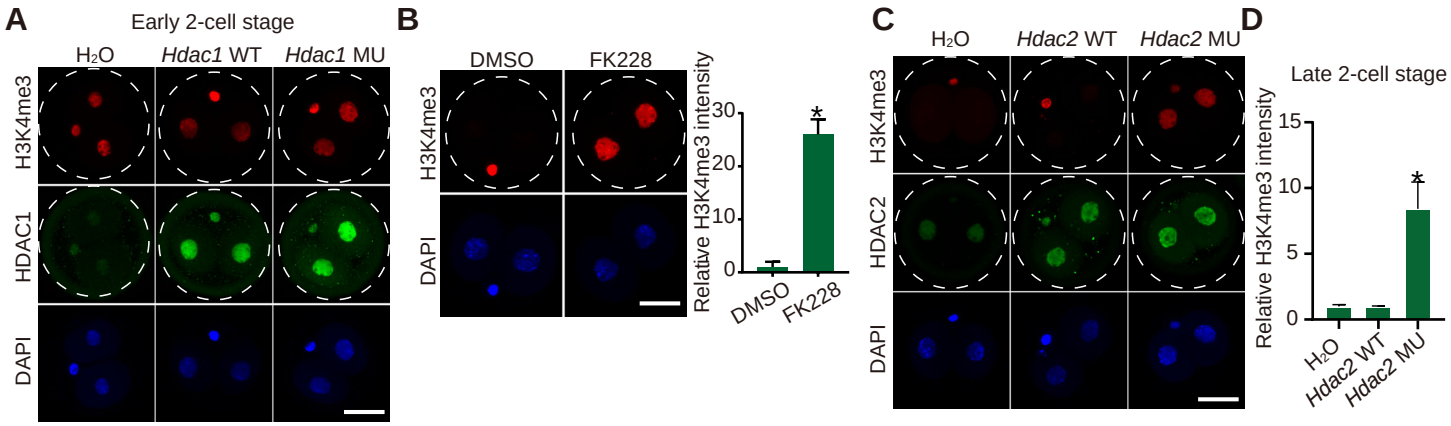

Fig. S6. HDAC1/2 is required for removal of H3K4me3 during ZGA. A, Immunofluorescence staining of H3K4me3 and HDAC1 in mouse embryos at early 2-cell stage. **B,** Immunofluorescence staining of H3K4me3 embryos at late 2-cell stage. Left, representative images, scale bar, 25 μm. right, H3K4me3 intensity relative to DMSO-treated embryos. Data shown as Means ± s.e.m. (n = 3; 3-7 embryos per group per replicate, *$P < 0.05$). **C,** Immunofluorescence staining of H3K4me3 and HDAC2 in mouse embryos at late 2-cell stage. **D,** H3K4me3 intensity relative to H_2O injection embryos. Data shown as Means ± s.e.m. (n = 3; 3-7 embryos per group per replicate, *$P < 0.05$ (MU vs WT or H_2O)).

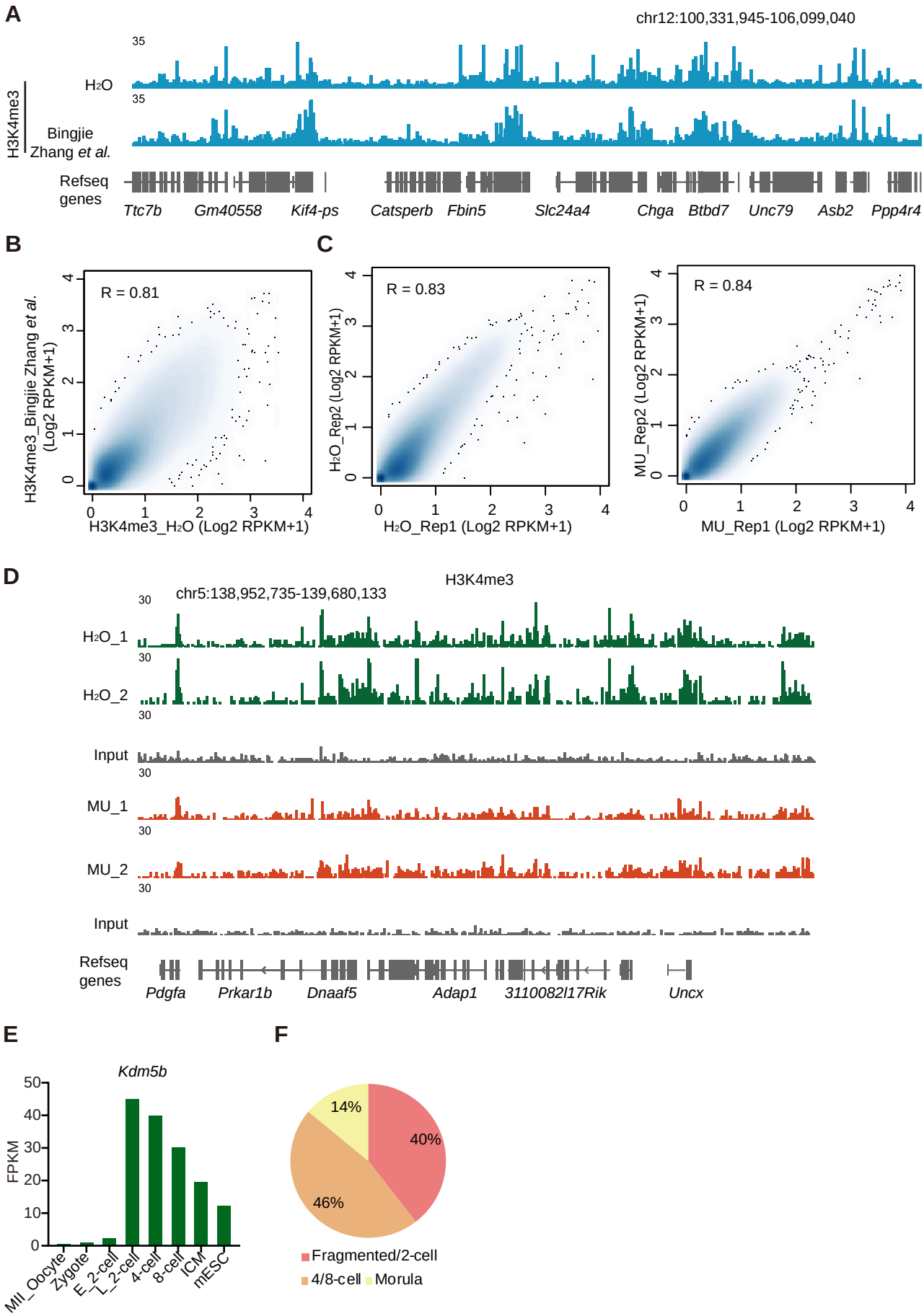

Fig. S7. H3K4me3 ULI-NChIP- seq validation. A, Browser snapshots of H3K4me3 in late 2-cell embryos injected with H_2O and published ChIP-seq data. **B,** Scatter plots showing the H3K4me3 signal (RPKM for 2-kb bin across the genome) in late 2-cell embryos between data sets in this study and Bingjie Zhang *et al*., R refers to Pearson correlation coefficient. **C,** Scatter plots showing the H3K4me3 signal (RPKM for 2-kb bin across the genome) between two biological replicates. **D,** Browser snapshots showing H3K4me3 signals in two biological replicates of embryos injected with H_2O or *Hdac1* mutant mRNA. **E,** Relative expression of *Kdm5b* in mouse oocytes, preimplantation embryos and mouse embryonic stem cells (mESCs). **F,** Distribution of cleavage embryos found in embryos injected with *Hdac1* mutant and *Kdm5b* mRNA at day 3.75 after fertilization.

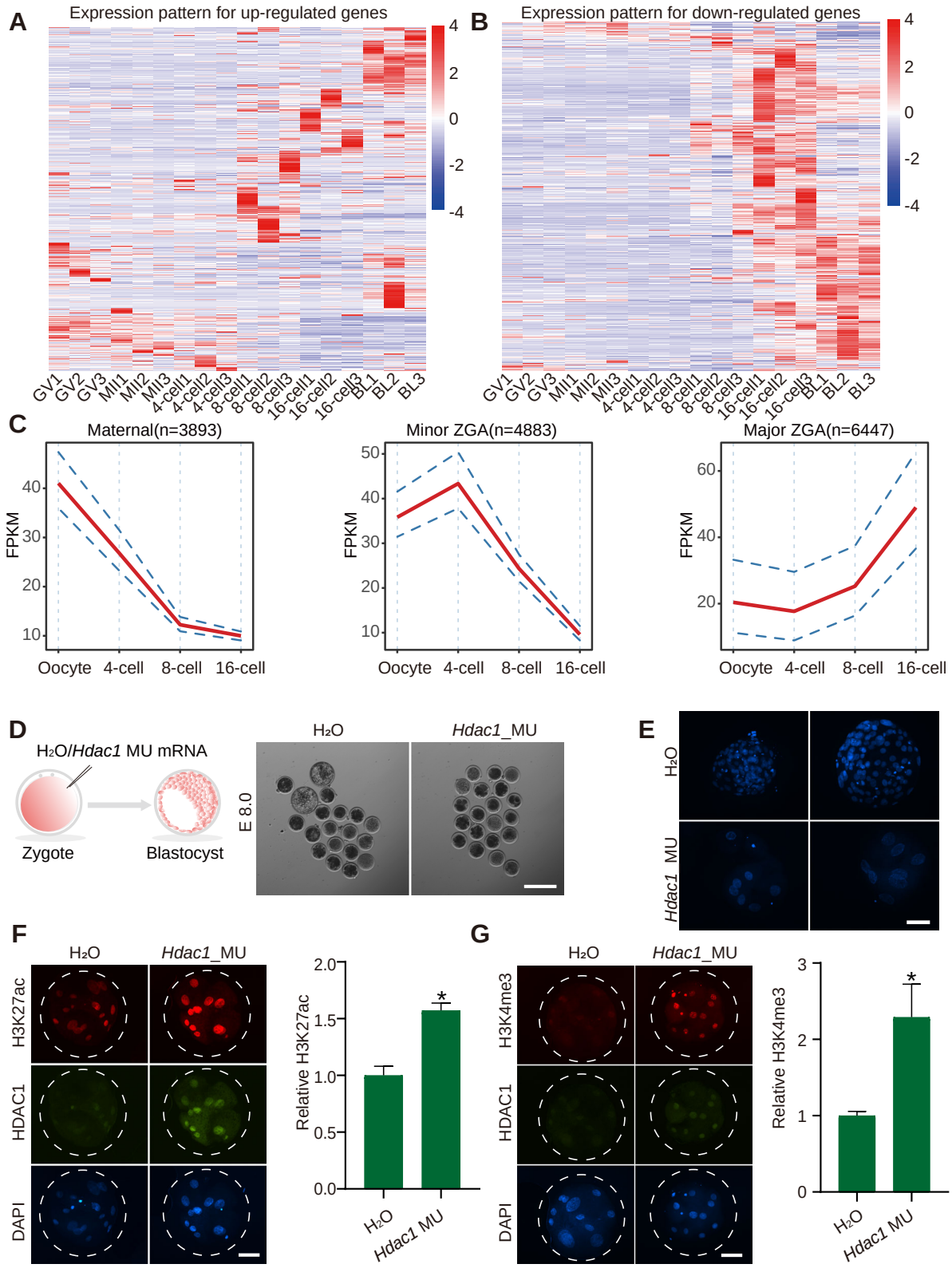

Fig. S8. HDAC1/2 is crucial for bovine ZGA. A and B, Expression pattern of all up-regulated genes (FK228/DMSO, A) and down-regulated genes (FK228/DMSO, B) in bovine oocytes and preimplantation embryos using published RNA-seq data(Graf et al., 2014). **C,** Three distinct gene expression patterns during bovine embryo development. The three gene categories are generated by *k-means* clustering of RNA-seq data(Graf et al., 2014) for bovine MII oocytes and 4-cell, 8-cell, 16-cell embryos and blastocysts. Red lines showing the average FPKM, and dashed blue lines showing 95% confidence interval around the mean. The number of genes in each cluster is also indicated in the brackets. **D**, Experimental scheme (left) for *Hdac1* MU mRNA injection and representative images in bright field (right) on day 8.0 after fertilization of bovine embryos. **E,** DNA staining with DAPI at day 8.0 after fertilization for bovine embryos. **F,** H3K27ac and HDAC1 immunofluorescence staining for bovine 8/16-cell embryos. Left: representative images, scale bar, 50 μm, right: H3K27ac intensity relative to H_2O-injected embryos. Data shown as Means ± s.e.m. (n = 3; 3-10 embryos per group per replicate, $*P < 0.05$). **G,** H3K4me3 and HDAC1 immunofluorescence staining for bovine 8/16-cell embryos. Left: representative images, scale bar, 50 μm, right: H3K4me3 intensity relative to H_2O-injected embryos. Data shown as Means ± s.e.m. (n = 3; 3-10 embryos per group per replicate, $*P < 0.05$).

Table S1. Antibody information

Name	Host	Company	Catalog Number	Application
HDAC1	Mouse	Cell Signaling Technology	#5356	IF (1:200)
HDAC2	Mouse	Cell Signaling Technology	#5113	IF (1:200)
H3K27ac	Rabbit	Active Motif	39133	IF (1:200)
H3K4me3	Rabbit	Cell Signaling Technology	#9751	IF (1:200)
Ser2P	Rabbit	Abcam	Ab5095	IF (1:200)
Donkey anti-Rabbit 594		Invitrogen	A21207	IF (1:100)
Goat anti-Mouse 488		Invitrogen	A11001	IF (1:100)

Table S2. Differentially expressed genes identified by RNA-seq between Hdac1 MU and Hdac1 WT mRNA injection group in mice late 2-cell embryos (ranked by adjusted padj). Threshold: padj <= 0.05 & FoldChange >= 2 or FoldChange <= 0.5.

Click here to download Table S2

Table S3. GO enrichment of up-regulated differentially expressed genes.

Click here to download Table S3

Table S4. GO enrichment of down-regulated differentially expressed genes.

Click here to download Table S4